Lawrence Berkeley National Laboratory
Recent Work

Title
APPLICATION OF THE ANNNI MODEL TO LONG-PERIOD SUPERSTRUCTURES.

Permalink
https://escholarship.org/uc/item/7jb2s4k1

Authors
Fontaine, D. de
Kulik, J.

Publication Date
1984-07-01

eScholarship.org Powered by the California Digital Library
University of California

LBL-18067
Preprint c.2

Lawrence Berkeley Laboratory

UNIVERSITY OF CALIFORNIA

RECEIVED
BERKELEY LABORATORY
AUG 20 1984
LIBRARY AND
DOCUMENTS SECTION

Materials & Molecular Research Division

Submitted to Acta Metallurgica

APPLICATION OF THE ANNNI MODEL TO LONG-PERIOD SUPERSTRUCTURES

D. de Fontaine and J. Kulik

July 1984

TWO-WEEK LOAN COPY

This is a Library Circulating Copy
which may be borrowed for two weeks.

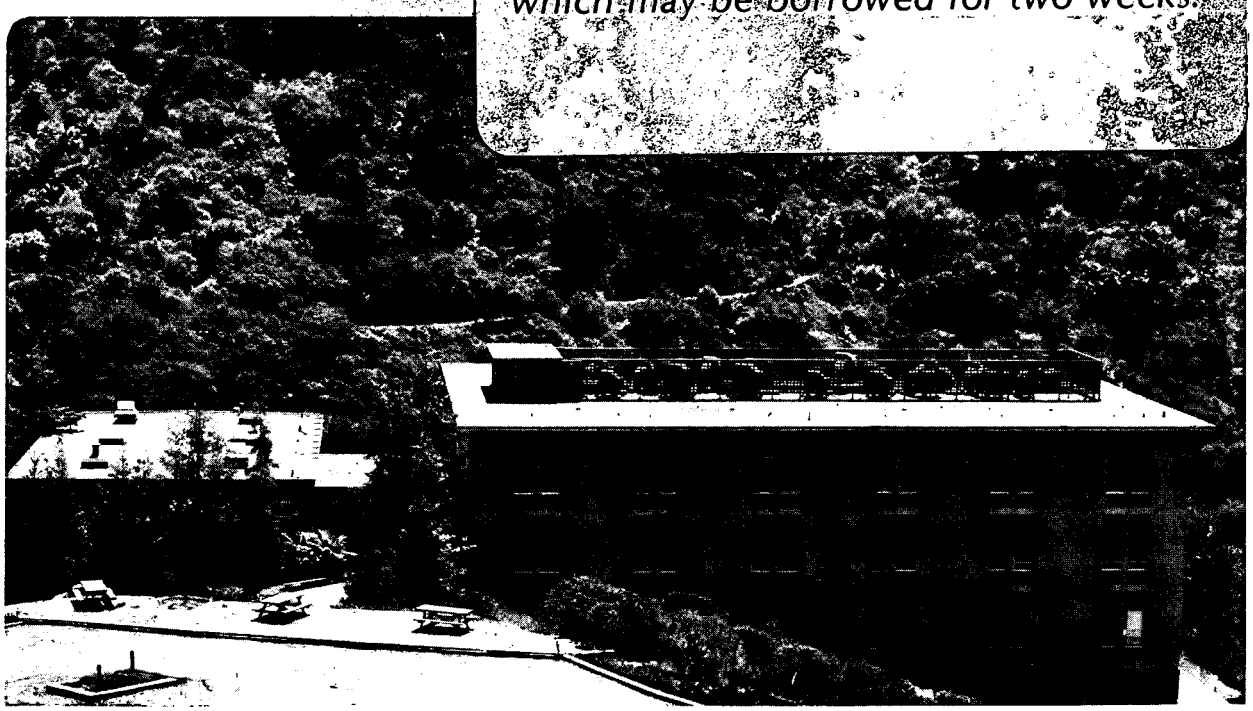

Prepared for the U.S. Department of Energy under Contract DE-AC03-76SF00098

LBL-18067 c.2

DISCLAIMER

This document was prepared as an account of work sponsored by the United States Government. While this document is believed to contain correct information, neither the United States Government nor any agency thereof, nor the Regents of the University of California, nor any of their employees, makes any warranty, express or implied, or assumes any legal responsibility for the accuracy, completeness, or usefulness of any information, apparatus, product, or process disclosed, or represents that its use would not infringe privately owned rights. Reference herein to any specific commercial product, process, or service by its trade name, trademark, manufacturer, or otherwise, does not necessarily constitute or imply its endorsement, recommendation, or favoring by the United States Government or any agency thereof, or the Regents of the University of California. The views and opinions of authors expressed herein do not necessarily state or reflect those of the United States Government or any agency thereof or the Regents of the University of California.

LBL-18067

APPLICATION OF THE ANNNI MODEL TO LONG-PERIOD SUPERSTRUCTURES

D. de Fontaine and J. Kulik

Lawrence Berkeley Laboratory
University of California
Berkeley, California 94720

July 1984

This work was supported by the Director, Office of Energy Research, Office of Basic Energy Sciences, Materials Sciences Division of the U.S. Department of Energy under Contract Number DE-AC03-76SF00098.

APPLICATION OF THE ANNNI MODEL TO LONG-PERIOD SUPERSTRUCTURES*

by

D. de Fontaine

University of California
Department of Materials Science and Mineral Engineering
Berkeley, California 94720

J. Kulik

University of California
Department of Physics

ABSTRACT

Existing models of long-period superstructures are re-examined in the light of the recently developed Axial-Next-Nearest-Neighbor-Ising (ANNNI) Model. In this model, long-period phases are contained in a triangular shaped phase diagram region bounded by a Lifshitz point on the uppermost transition temperature line and a multiphase point at zero absolute temperature. Periodic antiphase structures are produced by a square-wave modulation of the ordered ground state, resulting in new types of long-period superstructures, here denoted as "Fujiwara phases." The role of configurational entropy in stabilizing long-period phases is emphasized. The applicability of the ANNNI model to periodic antiphase structures in ordered alloys is examined, and the striking resemblence between predicted structures and those observed experimentally in Ag"$_3$"Mg and Au"$_3$"Zn is pointed out. The difference between "straight" and "wavy" (CuAu II) antiphase domain boundaries is discussed in the light of the model.

*This work was supported by the Director, Office of Energy Research, Office of Basic Energy Sciences, Materials Sciences Division of the U. S. Department of Energy under Contract No. DE-AC03-76SF00098.

1. INTRODUCTION

The stability of long-period superstructures has for years intrigued many investigators. In particular, the fact that well-defined ordered sequences of one or two-dimensional patterns repeat regularly over long distances appears to require very long-range interactions, the origin of which remained a subject of some controversy.

The currently accepted explanation for the stability of such structures in ordering systems is the one first proposed by Sato and Toth *[1]*, and later modified by Tachiki and Teramoto *[2]*. More recently, the problem has been considered by Vul and Krivoglaz *[3]*. The Sato and Toth (ST) theory is based upon the idea that a periodic *modulation* of the structure introduces new Brillouin Zone boundaries, thereby lowering the electronic energy if these zone boundaries fall close to flat portions of the Fermi surface. Good experimental agreement with theory was found by ST *[4]* on vapor-deposited thin films of alloys of various compositions. Very recently, Gyorffy and Stocks *[5]* have performed KKR-CPA computations of the Fermi surfaces in Cu-Pd alloys of different average concentrations. The calculated Fermi surfaces exhibited rather flat portions separated by distances $2k_F$ in the <110> directions which, when introduced in the ST formalism, predicted values of long-period wavelengths in good agreement with those found experimentally.

Thus, the ST Fermi-surface theory would appear to be well substantiated, were it not for the fact that, since the model is based solely on electronic energy minimization, at least in its original form, it contains no in-built temperature dependence, no configurational entropy

effects. It might then be argued that the model should be valid only at low temperatures; but it is precisely in those regimes that the ST theory fails most conspicuously: as will be recalled in Sect.5, long-period superstructures are often found in intermediate temperature ranges, and tend to disappear at low temperatures.

Recently, a radically different model has been proposed to explain the phenomenon of periodically modulated *magnetic* order in certain rare earths, particularly in CeSb. This model, already proposed in 1961 by Elliott *[6]*, now goes under the designation of ANNNI model, for *Axial Next Nearest Neighbor Ising* model *[7,8]*. As the name implies, the model, recently reviewed by Selke *[9]*, makes use of a very simple Ising Hamiltonian with nearest (nn) and next-nearest neighbor (nnn) interactions along a single "axial" direction. Mean-field theory *[7,10,11]*, soliton theory *[11,12]*, Monte Carlo simulations *[13]*, and low-temperature expansions *[8,14]* are used to find approximate solutions to the three-dimensional Ising problem. Configurational entropy effects are displayed prominently, but no effort is made to evaluate the near-neighbor interaction parameters which appear in the Hamiltonian. It will be argued below, however, that the Fermi-surface and ANNNI models are by no means mutually exclusive.

We begin, in Sect. 2, by defining what we mean by the term *modulated structures*, which requires a slight extension of the classical notion of *phase*. A phenomenological description of such phases is proposed in Sect. 3, whilst a thermodynamical treatment is intoduced in Sect. 4. Possible applications to well-known ordering systems are then discussed in Sect. 5.

2. MODULATED PHASES

Let us consider crystals which are sufficiently anisotropic that their ground states can be described as a stacking of perfectly ordered layers normal to a unique *axial* direction. The layers can disorder progressively at higher temperatures, of course, but, below the highest transition temperature, it must always be possible to label each layer unambiguously by a single symbol: + or -, say. The {+,-} sybols might designate, for example, {spin-up, spin-down}, {A,B} atoms, {unshifted ordered layer, shifted ordered layer}, etc.. Layers could – but need not – be individual lattice planes, their stacking pattern creating a one-dimensional *modulation* of layer-averaged magnetization, composition, degree of order, etc.. When the modulation is perfectly periodic, a true *long-period superstructure* results.

It is well known that electronic or elastic effects can lead to long-wavelength modulations. To develop a tractable statistical thermodynamical model, it is necessary to map these actual *physical* interactions onto a small set of *effective* near-neighbor pair interactions. Specifically, we shall consider single nn interaction J_0 within the layers, and two *axial* interactions, J_1 and J_2 for the nn and nnn neighbor interactions, respectively, in the direction perpendicular to the layers. Such is essentially the ANNNI Model.

It is of considerable interest to determine what long-period superstructures may be stable under what conditions and in what temperature ranges; in other words, one would like to determine the *phase diagram* for this model. The vertical axis traditionally represents the temperature, the

horizontal axis (axes) representing an external magnetic field, a chemical potential, or some other physical parameter. In the present study, all phase diagrams will be plotted in a (T,κ) plane, where T is the absolute temperature and $\kappa=J_2/J_1$ is the ratio of axial pair interactions. Vanishing applied field, either magnetic or "chemical", will always be assumed.

Features common to many ANNNI phase diagrams are indicated schematicallly in Fig. 1. Four main phase regions are represented: a high-temterature disordersd (D) phase (more symmetric, sometimes designated as "normal" or "paramagnetic"), an ordered phase (O_1) of "simple" structure (less symmetric, "ferromagnetic" or "antiferromagnetic"), another somewhat more complex ordered phase (O_2), characterized by a modulation wavelength of four times the layer spacing, and, occupying a central position between those three phase regions, that of the *modulated phases* (Mod).

Two especially interesting points are found in the phase diagram of Fig. 1 (excluding the one at infinity, L_∞): a multicritical point called *Lifshits point* at L, at which a disordered, an ordered, and a "modulated phase" come together, and a multiphase point of infinite degeneracy of ground states at T=0, at a critical value κ_0 of the competing interaction parameter ratio of J_2 to J_1. Recent theoretical studies, to be summarized in Sect. 4, have made systematic use of those two points in elucidation the nature of the transition to the modulated phases, mainly by performing (a) a Landau expansion about the Lifshits point L, and (b), a low-temperature expansion about the multiphase point κ_0. Unfortunately, there exists no tractable mathematical model valid for the whole T and κ ranges; the global phase diagram has to be assembled in a somewhat fragmentary fashion.

Actually, the region labeled "Mod", is composed of infintely many commensurate and incommensurate phase regions, but, before going further,

it is necessary to define operationally the words *commensurate* and *incommensurate*. To that end, consider a perfectly periodic modulation of half-wavelength

$$\lambda/2 = Md \quad , \tag{1}$$

measured by the dimensionless number M in units of the interlayer spacing d. Mathematically, the modulation period is *commensurate* with the one-dimensional lattice of layers if

$$M = P/Q \qquad (P > Q) \quad , \tag{2}$$

where P and Q are relative primes. The period is incommensurate if M cannot be expressed as a rational number. It is seen, by Eqs. (1) and (2), that modulation and lattice will be in registry at multiples of the interval

$$\Lambda = Pd = Q\lambda/2 \quad . \tag{3}$$

The integer P will be called the *commensuration number*, the *commensuration wavelength* being equal to Λ when the integer Q is even, and 2Λ when Q is odd. Examples will be given in the next Section. The set of rational fractions 1/M has measure zero in the set of real numbers in the [0,1] interval, hence, if all values of M were equally probable, incommensurate periods would be infiniltely more densely distributed than commensurate ones *[15]*. Actually, because of coupling effects between the modulation and the lattice, there will be a tendency for the modulation period to *lock in* at well-defined commensurate values, particularly at low temperatures. These points will be discussed further in Sect. 4.3.

Commensurate long-period superstructures can be considered as crystallographic phases with very long unit cells, or *polytypes*. When the modulation half-wavelength evolves from one commensurate value to the next (as temperature, or composition or κ varies), the space group of the corresponding polytype changes, if for no other reason that translational

symmetry elements are gained or lost in the process. Hence, a definite phase boundary *must* exist on the phase diagram between successive *commensurate phases*. Thus, at least in those regions where the lock-in tendency is weak, the diagram of Fig. 1 in the Mod region may consist of infinitely many commensurate phase regions, often of extremely narrow extent.

Clearly, it is not possible to determine the phase fields of all such commensurate structures: resolution, theoretical or experimental, is finite; furthermore, since the driving force for transforming from one commensurate long-period superstructure to the next one must become very small as the commensuration number P becomes large, equilibrium will be practically impossible to achieve for polytypes with very narrow phase fields. It thus becomes imperative to adopt a more practical though less mathematical definition of commensurate/incommensurate periods: *a commensurate long-period structure shall be that whose half-period can be expressed as $M=P/Q$, P and Q being small relative primes*. For example, a fixed upper limit P_{max} might be imposed on the commensuration number P. According to this practical definition, one thus expects to find, in some parts of the phase diagram, commensurate phase fields separated from each other by incommensurate phase regions in which the period M can apperar to vary continuously. Thermodynamically, of course, phases with modulation period varying by finite amounts are not allowed, this possibility existing here only as an artefact of the operational definition adopted for the word "commensurate".

Long-period superstructures will now be examined in more detail.

3. CHARACTERISATION OF SUPERSTRUCTURES

The essential features of diffraction patterns obtained from long period superstructures will be briefly reviewed in Sect. 3.1, along with the interpretation thereof. More direct evidence obtained by high-resolution electron microscopy will be described in Sect. 5. A remarkable feature of all long-period superstructures resulting from square-wave modulations of a one-dimensional lattice will be presented in Sect. 3.2 and in Appendix I.

3.1. Diffraction Patterns

Only the briefest diffraction treatment will be given here. For details concerning, say, which superlattice reflections are associated with periodic antiphase satellites, or concerning the way the phases of Fourier amplitudes contribute to satellite intensity, or concerning possible disordering and displacement effects, the reader is referred to the work of Perio and collaborators *[16,17]*.

For simplicity, only one-dimensional modulations will be considered. Let x be a continuous variable in the direction of the modulation. Atomic layers - such as lattice planes, single or double - are placed normally to the x axis at equidistant points

$$x_p = pd \qquad (p=0,1,2,...N-1) \quad ,$$

d being the inter-layer spacing, and N being the total number of layers. Now define a *modulating function* f(x) of the continuous variable x which imparts to each pth layer the value $f_p = f(x_p)$ for the physical parameter considered, be it composition, degree of order, "antiphasing" or

magnetization.

In the kinematic approximation, the diffracted amplitude per layer due to the modulation is proportional to *[18]*

$$A(k) = \frac{1}{N} \sum_{p=0}^{N-1} f(x_p)\, e^{-ikx_p} \tag{3}$$

where k is a discrete variable having reciprocal space values

$$k = \pm 2\pi h/d \tag{4}$$

with Miller index

$$h = H/N \qquad (H=0,1,2,\ldots). \tag{5}$$

Equation (3), which is assumed to contain implicitly the scattering power of the modulation f, can also be written

$$A(k) = \frac{1}{N} \sum_p \left[\int F(K)\, e^{iKx_p}\, dK\right] e^{-ikx_p} \tag{6}$$

where F(K) is the Fourier transform of the modulating function f(x). In Eq. (6), the integration is performed over an appropriate region of continuous reciprocal space. The expression $\Sigma_p \exp[-i(k-K)x_p]$ in Eq. (6) yields a set of *scattering functions* with sharp peaks of height ±N at all values of the argument k-K equal to a reciprocal lattice vector $g_H=2\pi H/d$ of the layered structure, H indicating the order of the reflection. The scattered amplitude is then proportional to

$$A(k) = \Sigma_p\, sF(k-g) \tag{7}$$

where s, a factor of modulus unity, takes care of the shape and sign of the scattering functions.

Now let the modulating function be periodic of period 2Md. Its Fourier transform then consists of a set of δ functions of weight C_n at

K-space positions

$$K_n = \pm\pi n/Md \qquad (n=0,1,2,\ldots). \tag{8}$$

The resulting satellite amplitude spectrum, by Eqs. (7) and (8), appears as a convolution of the Fourier harmonics of f(x) with the reciprocal lattice of the layers:

$$A(k) = \sum_H \sum_n sC_n\ \delta(k-g_H+K_n). \tag{9}$$

In general, sharp satellite reflections will thus be found at positions

$$h = H + n/2M = \frac{2HP + nQ}{2P} \tag{10}$$

where, as in Eq. (2), P and Q are relative primes. Satellite reflections will therefore be placed 1/2P apart (in 1/d units), so that the satellite spectrum can become infinitely dense when the commensuration period 2P becomes very large. In practice, satellite intensity

$$I(k) = |A(k)|^2$$

will decrease rather rapidly with the reflection order, so that only a few peaks will be observed about each fundamental H. An apparently uneven satellite spacing may then result, as explained below for the case of a square wave modulation.

Among the better-studied modulated structures, both by X-ray diffraction and transmission electron microscopy, are the so called *periodic antiphase structures*. These are found typically in ordered alloys in which antiphase boundaries occur at regular intrvals, in one and two dimensions. Here, only one-dimensional *conservative* periodic antiphase structures will be considered. Evidence suggests that, in many ordered

systems, the modulating function f(x), which fixes the location of the antiphase boundaries, can be idealized as an almost perfect square wave. Hence, f(x) must have a Fourier spectrum consisting only of odd harmonics at $\pm(2m+1)/2M$, with intensities decaying as $(2m+1)^{-2}$, (m=0,1,2...). The decay law of the satellites themselves will be somewhat different because, by Eq. (9), higher harmonics can contribute to all satellite orders.

For commensuration number P finite, no matter how large, the modulation satellites can be regarded as fundamental reflections of the correponding *polytype* of long unit cell 2Pd in the direction of the modulation. Hence, as can be also inferred from Eq. (10), it is the number 1/2P, rather than 1/2M, which fixes the satellite spacing, a conclusion which is not apparent in the early work of Fujiwara *[18]*, but which was clearly stated in that of Perio and Tournarie *[16]*. Two additional factors must be taken into account in analysing satellite spectra: systematic extinctions and gradual intensity decay with harmonic order. For example, if Q is odd, then the numerator on the right side of Eq. (10) is also odd, and satellites can only occur at odd multiples of 1/2P; if Q is even, then P must be odd, and satellites will occur at all multiples of 1/P. Furthermore, as mentioned above, harmonic intensity decay will cause higher-order satellites to be practically invisible, thereby resulting in apparent unevenness of spacing in each reciprocal unit cell and precluding unambiguous determination of P and Q.

This latter effect will be particularly noticeable for modulations of large commensuration number P. As an illustration, consider the three following polytypes whose structures (to be described in the next sub-section) are similar, and whose half-periods are:

(a) $M = 25/14 = 1.7857...$

(b) $M = 67/14 = 4.7857...$

(c) $M = 9/5 = 1.80$.

The correponding spectra are indicated in Fig. 2 a,b,c. In this schematic representation, the diameter of the spots represent approximate relative intensity, i.e. the most intense spot corresponds to the first harmonic of the modulating square wave, the next intense to the third harmonic, etc... It is seen that, in case (a), 23 harmonics are necessary to occupy all satellite positions predicted by Eq. (10) – after that, intensities of still higher orders begin to superimpose – wereas in case (b), after the same number of harmonics, the spacings are still irregular: 65 harmonics would be necessary to produce an even spacing.

The observation that satellite sequences do not "mesh" at the Brillouin Zone boundary (h=0.5) has sometimes been taken as a criterion for "incommensurability" *[19]*. From the foregoing, however, it is clear that such a criterion is, at best, a relative one: in case (a), if all 23 orders are observed, the structure would be said to be *commensurate*, if only 9 orders are observed, for example, the structure would be classed as *incommensurate*. Case (c), with 9 orders observed, would be a *commensurate* structure.

Nevertheless, these observational considerations, far from infirming the practical commensurability criterion proposed in Sect. 2, actually provides a convenient estimate of P_{max}, the commensuration number beyond which a modulation is defined operationally as being incommensurate. Since, as can easily be shown, the satellite spectrum is "complete", in the sense of Eq. (10), when harmonics of up to order $n=2m+1=P$ (or $P-1$) have been used up, then P_{max} may be set equal to n_{max}, the maximum harmonic order which will significantly contribute to the satellite intensities. In the

above examples, if $n_{max}=23$, both modulations (a) and (c) will be commensurate, (b) incommensurate; if $n_{max}=9$, only (c) will be commensurate.

3.2. Square Wave Modulation

Consider the case of an observed satellite intensity spectrum which is consistent with a perfect square wave modulation f(x) of half-period M=P/Q. The effect of this modulation on the layer lattice is then quite straighforward to interpret: any layer of index p can then be assigned unambiguously the sign + or - according to the parity of the integer

$$q_p = [pQ/P + \epsilon] \quad , \qquad (11)$$

representing the largest integer contained in the bracketed expression. In Eq. (11), the rational fraction ϵ allows for an arbitrary shift of the square wave origin with respect to that (p=0) of the layer lattice. Fujiwara *[18]* showed that the layering sequence resulting from a square wave modulation of half-period M = 9/5 = 1.80 [example (c), above] was as follows:

$$(2\bar{2}2\bar{2}1\bar{2}2\bar{2}2\bar{1}....) \quad , \qquad (12)$$

a symbolic notation signifying: two "+" layers, followed by two "-" layers, ... followed by a unique "+" layer, followed by two "-" layers, etc... In what follows, the short-hand notation of Fisher and Selke *[8]* will be adopted for describing such sequences: $\langle 2^4 1\rangle$, in which angle brackets indicate a repeating period (or half-period).

Fujiwara gave other examples of layer arrangements, such as

$$(2\bar{2}2\bar{1}2\bar{2}1\bar{2}2\bar{1}\ldots) \quad , \qquad (13)$$

which also produced sharp satellites at positions $h = H \pm (2m+1)/2M$, with intensity decreasing roughly as $(2m+1)^{-2}$. Fujiwara descibed layerings such as those given by formulas (12) and (13) in the following terms:

(i) Regular arrangements with uniform mixing.

Other arrangements were also considered by him:

(ii) Regular arrangements with non-uniform mixing

(iii) Irregular arrangements with almost uniform mixing

(iv) Irregular arrangements with non-uniform mixing.

Arrangements (ii) and (iv) were shown to produce specra not in agreement with observation, although some degree of "irregularity", as in (iii), could still yield acceptable spectra.

Fujiwara's terminology can be translated into the present one as follows:

Regular arrangement → perfect commensuration period 2P

Uniform mixing → perfect modulation periodicity 2M.

Although it was not stated by Fujiwara explicitly, it is clear from the diffraction equations recalled above that the idealized periodic antiphase structures which produce sharp satellite intensity at the correct positions are those which result from a modulating square wave of perfect periodicity. It does not matter in the least that the modulating wave be a function in fictitious, *continuous* x-space, with period 2M totally unrelated to that of the layers, the latter existing in real, *discrete* x_p-space. Clearly, it is the "regularity" of the modulating function itself which produces proper satellite spectra, it is the nature of f(x) which determines the arrangement of layers.

It is then of interest to inquire into the structural properties of the polytypes which result from general square-wave modulations of perfect period 2M. It is desired to construct an algorithm for obtaining explicitly one half-period of the layering sequence given by Eq.(11). Surprisingly, the required algorithm is precisely the one derived independently in 1978 by Hubbard *[20]* for the case of electrons occupying the sites of a one-dimensional lattice in an organic conductor such as TTF-TCNQ, and by Pokrovsky and Uimin *[21]* for the case of ad-atoms occupying the sites of a one-dimensional substrate lattice. In both cases, electrons or ad-atoms are assumed to interact with long-range repulsive *convex* pair interactions, such as those resulting from a Coulomb potential. The ratio (<1) of interacting particles (electrons or ad-atoms) to the number of lattice sites is fixed. The algorithm will now be described in the (slightly modified) notation of Hubbard *[20]*.

First, one must expand the rational half-period M in a continued fraction

$$M = \frac{P}{Q} = n_0 + \cfrac{\gamma_0}{n_1 + \cfrac{\gamma_1}{n_2 + \cfrac{\gamma_2}{\ddots \; n_{k-1} + \cfrac{\gamma_{k-1}}{n_k}}}} \tag{14}$$

Since M is a rational fraction, the continued fraction expansion must terminate at some level, say k. At any level i, the integers n_i are determined uniquely by the remainder (r) at level i-1 :

$$1/r_{i-1} = n_i + \gamma_i r_i \tag{15}$$

with

$$-1/2 < r_i \leq +1/2$$

so that

$$\gamma_i = r_i/|r_i| = \pm 1 \quad . \tag{16}$$

Now define the sequences {X} and {Y} by the recursion formulas

$$X_o = n_o \tag{17a}$$

$$Y_o = n_o + \gamma_o \tag{17b}$$

$$\left.\begin{aligned} X_i &= (X_{i-1})^{n_i-1}\, Y_{i-1} \quad (17c) \\ Y_i &= (X_{i-1})^{n_i+\gamma_i-1}\, Y_{i-1} \quad (17d) \end{aligned}\right\} \quad (i = 1,2,..,k-1) \ .$$

The formula for polytype of half-period M is then

$$\langle X \rangle = X_k \quad . \tag{18}$$

A proof that this algorithm indeed yields the correct polytype structures resulting from a square wave modulation is given in Appendix I, along with a numerical example. All polytypes (X) thus generated will henceforth be called *Fujiwara (FW) phases* for short. The three square-wave modulations whose spectra are illustrated in Fig. 2 have symbolic formulas

(a) $\langle (2^4 1)^2 2^3 1 \rangle$,

(b) $\langle (5^4 4)^2 5^3 4 \rangle$,

(c) $\langle 2^4 1 \rangle$.

Other examples will be found in Table I which lists all FW phases with P=73 and 1.5<M<2, and in Table II which lists all FW phases with commensuration number P<20, for the same range of modulating period. Table II also indicates the level k at which the continued fraction terminates. The structural formulas given in Tables I and II were calculated directly from Eq. (11) with $\epsilon = 0$. As explained in Appendix I, the resulting polytype formulas may differ in appearance from those derived from the continued fraction algorithm, but both are completely equivalent, due to the translational symmetry of the long-period structures.

It follows fron Eqs. (14) to (18) that all FW phases consist of, say, α units of type $X_o^j Y_o$ and β units of type $X_o^{j-1} Y_o$. The total number of both types of units is then

$$S = \alpha + \beta \tag{19}$$

and the total number of "domains", or square-wave modulation half-periods is

$$Q = j(\alpha+\beta) + \alpha \quad . \tag{20}$$

Hence the half-period of the modulation must be equal to

$$M = X_o \pm S/Q \quad , \tag{21}$$

the sign being taken in accordance with that in Eq. (16). The fractional part of M thus depends only on the repetition numbers j, α, and β, and not on the domain lengths X_o and Y_o. Examples (a) and (b), above, illustrate the latter property. The fraction P/Q itself, of course, is equal to the total number of layers in the polytype's structurel formula divided by the total number of X_o and Y_o units contained therein, i.e. by the sum of the "exponents" in the formula.

3.3. Smooth-Profile Modulation

It is often observed experimentally that the satellite intensity decreases faster with order m than the $(2m+1)^{-2}$ law characteristic of square wave modulation. One then readily concludes that the modulating function f(x) must have a profile smoother than that of a square wave. In the limit, the modulation could be purely sinusoidal.

It is not clear *a priori* how a smooth profile is to be interpreted physically. The uncertainty results from the fact that (complex) satellite

amplitudes are not observable, only intenstites. Recently, however, high-resolution transmission electron microscspy has helped resolve some of the ambiguities of interpretation. In particular, it appears from the work of Guymont *et al.* *[19]*, that the periodic antiphase structure of CuAu II presents wavy aniphase boundaries, whereas those of Ag_3Mg, for example, are perfectly staight. The observed difference between these two fcc-based ordered systems has led these authors to conclude that the Fujiwara (FW) model is applicable to the Ag_3Mg case, whilst the Jehanno and Perio (JP) model *[17]* might be more applicable to the CuAu case.

Formally, it is merely required to look upon the Ag_3Mg long period superstructures as resulting from a square wave modulation (giving rise to the *FW phases* described in the previous section), those of CuAu then resulting from a modulation "with corners rounded off". The representative smooth function f(x) must then represent an *antiphasing probability*, interpreted as the projection of actual antiphase shifts along the axial direction of the long period. Such is, of course, the JP model, but in the present view, both FW and JP models derive from the modulating function f(x), being merely distinguished from one another by the sharpness of the profile.

The most likely interpretation of a smooth profile is illustrated in Fig. 3, drawn so as to resemble schematically high-resolution TEM micrographs of typical CuAu II samples *[22]*. Segments of Cu (light) and Au (dark) (001) lattice planes are shown stacked along the vertical direction, with antiphase shifts occurring approximately every five (100) lattice spacings. Random errors have been introduced for the positions x at which these phase shifts take place, resulting in the *projected* antiphasing modulation f(x) shown just below the schematic representation of the

structure. Such an interpretation was already proposed by Jones *[23]* and by Portier and Gratias *[24]*.

It is apparent that the "staggered domain" configuration depicted in Fig. 3 leads to "wavy" antiphase domain boundaries as observed by Guymont *et al.* *[22]*. Indeed, it will be argued in the next section that this "wavyness" could be the result of an *interface roughening transition*. Such a transition is quite apparent in Monte Carlo simulations carried out by Selke and Fisher *[13]*. Note that, whether antiphase boundaries are straight or wavy, i.e. whether the projected profiles f(x) have sharp or diffuse interfaces, satellite intensity should remain quite sharp as long as the modulating function is perfectly periodic.

4. THERMODYNAMICS OF SUPERSTRUCTURES

Two regions of the schematic ANNNI model phase diagram of Fig. 1 have been investigated in some detail: that in the neighborhood of the Lifshitz point L and that in the neighborhood of the multiphase point κ_0. Recent results pertaining to those two regions will be summarized in Secs. 4.1. and 4.2., respectively. A complete, albeit schematic, phase diagram will be presented in Sect. 4.3.

4.1. Lifshitz Point

The presence of long-period modulations near a second-order transition are intimately linked to the existence of the so-called "Lifshitz point," a term coined by Hornreich, Luban and Shtrickman *[25]*. These authors defined the new type of multicritical point in the following terms (slightly modified to conform to present notation) *[26]*: *the Lifshitz point is a multicritical point which divides a line of second-order transitions into two segments on one of which the equilibrium order parameter is characterized by a fixed wave vector* k^0, *allowed by the Lifshitz condition, whilst on the second,* k *varies continuously from* k^0 *as a parameter, in the present case* κ, *is changed. The L point is also the terminus of a second line in the T-*κ *plane which separates the ordered phases into two regions, one with* $k=k^0$ *and the other with* $k=k^*\neq k^0$.

Let us assume that the free energy F of a cystalline solid solution in an arbitrary state of partial order in the vicinity of a transition has the Landau expansion *[27]*

$$\Delta F = F_2 + F_3 + F_4 + \ldots, \tag{22}$$

where ΔF is the difference between F and its value in the disordered state and F_n is the nth order term in the expansion, expressed as a configuration-independent coefficient times the product of n concentration wave amplitudes Γ, taken as order parameters *[28,29]*. The first-order term vanishes at equilibrium and therefore does not appear in Eq.(22). The second order term has a particularly simple form *[29]*:

$$F_2 = \frac{N}{2} \sum_k F''(k)|\Gamma(k)|^2, \tag{23}$$

where N, the number of lattice planes and k, the wave vector have been defined earlier in Eqs.(3)-(5). For simplicity, as in Sect. 3.1, only one-dimensional concentration variations will be considered, in the axial direction of the modulation. The coefficient F" is the second derivative of the free energy with respect to concentration-wave amplitude squared, evaluated in the disordered state. In the present study, F" will be regarded as a known function of two intensive parameters

$$F'' = \Phi(T,\kappa;k) \tag{24}$$

with T the absolute temperature and κ the ratio J_2/J_1 of two effective pair interactions, for example.

Let us further assume that the disordered phase (D, in Fig.1) can transform by a second-order transition to the ordered (O_1) and modulated (Mod) phases. The case of first-order transitions is more difficult to

handle, and has not yet been treated in detail. In the second-order case then, the transition normally occurs at the vanishing of the coefficient F" evaluated at the wave vector k^o of the relevant ordering wave *[27]*. The Lifshitz condition restricts k^o to so-called "special points" *[28,29,30]* in reciprocal space, at which two or more symmetry elements intersect at a point *[27]*. At these points, any function of k having the symmetry of the disordered state's crystal structure, in particular the function $F'' = \Phi(k)$, must exhibit a local maximum, minimum or saddle point *[28]*.

Any regular function having the proper k-space symmetry can be written as a sum of trigonometric functions times appropriate coefficients, ω_n, say. In one dimension, the functional form is a very simple one:

$$\Phi = \omega_o - \omega_1 \cos 2\pi h - \omega_2 \cos 4\pi h - \ldots , \qquad (25)$$

the coefficients ω_n being themselves functions of T and κ. In Eq.(25), h is the Miller Index in the axial direction as defined by Eqs.(4) and (5). In a general Bragg-Williams (mean-field) approximation, the coefficients ω_1, $\omega_2 \ldots$ would be constants proportional to, respectively, $J_1, J_2 \ldots$, the effective pair interaction parameters, whilst ω_o would be simply proportional to temperature *[29]*. According to more general free energy models, such as the Cluster Variation Model (CVM) *[31]*, the values of the coefficients ω must result from the minimization of the free energy at each T and κ, and must therefore depend on these variables. Generally, the CVM free energy minimization must be performed numerically *[32]*. In simple cases, however, such as in the one-dimensional Ising chain with nearest-neighbor interactions (J_1), the (exact) result of the CVM minimization shows that ω_1 is proportional to k_BT times the hyperbolic

tangent of J_1/k_BT, k_B being Boltzmann's constant *[32]*. If both first and second neighbor interactions are included in the Ising chain, the second derivative F" takes the form (25), limited to three terms (as shown) with the coefficients $\omega_0, \omega_1, \omega_2$ now being rather complicated algebraic expressions involving the exponentials of J_1 and J_2 divided by k_BT *[33]*. Expressions for ω_1 and ω_2 must be asymptotic to J_1 and J_2, respectively, in the limit of high temperatures. In the qualitative analysis that follows, we shall therefore regard the expansion (25) as limited to the indicated first three terms, with ω_1 and ω_2 behaving roughly as J_1 and J_2 in the neighborhood of the critical temperature T_c, provided that J_1/k_BT or J_2/k_BT are not too large.

Since the second-order transition T_c occurs at the vanishing of the second derivative F", it is necessary to determine at which values of k (or h) Φ takes on its minimum values. For the simple form of Φ adopted, extrema occur at

$$\omega_1 \sin 2\pi h + 2\,\omega_2 \sin 4\pi h = 0,$$

i.e. at values of h which satisfy

$$\sin 2\pi h = 0 \tag{26a}$$

and

$$\cos 2\pi h = -\frac{\omega_1}{4\omega_2}, \tag{26b}$$

Equation (26a) yields all "Bragg peaks" at

$$h = 0,\ 1,\ 2,\ \ldots$$

and the "superlattice peaks"

$$h = \frac{1}{2},\ \frac{3}{2},\ \ldots\ .$$

Such are the "special-point extrema," the positions of which satisfy the Lifshitz condition *[27]*. The corresponding wave vectors will be designated by the symbol k^o (or h^o), regardless of whether the corresponding modulation is of "clustering (ferromagnetic) type" (integral values of h) or of "ordering (antiferromagnetic) type" (half-integral values of h).

Accidental extrema of the function Φ can also be found at values of h which satisfy Eq.(26b), provided that $\omega_1/4\omega_2$ be smaller than one in magnitude, i.e. for

$$\chi = \omega_2/\omega_1 \geq 1/4 \qquad (27a)$$

if ω_1 and ω_2 have same sign, and

$$\chi \leq -1/4 \qquad (27b)$$

if ω_1 and ω_2 have opposite sign. It is clear from Eq. (25) that special point (SP) extrema at integral values of h correspond to actual minima if ω_1 is positive ("clustering" or "ferromagnetic" case, $J_1>0$), whilst SP extrema at half-integral values are minima of Φ if ω_1 is negative ("ordering" of "antiferromagnetic" ase, $J_1<0$). It is also clear from Eq.(25) that accidental <u>minima</u> occur in both cases only if ω_2 is negative, from which one normally expects J_2 to be negative as well. In Sect. 4.2., it will appear that the condition for the existence of long period modulations at very low temperatures is expressed by $|J_2|/|J_1| \geq 1/2$, whereas, in the mean field (BW) approximation, the condition for the existence of accidental minima, leading to long-period modulation, is expressed by $|J_2|/|J_1| \geq 1/4$, according to Eqs.(26a,b). This discrepancy indicates that, although the BW model may yield approximately correct results at reasonably high temperatures, it cannot be relied upon near zero absolute.

In Sect. 4.2, it will also be seen that $|\kappa|=1/2$ locates the

multiphase point κ_o at 0^oK beyond which longer-period ground state structures (O_2) are expected. It will now be shown that

$$|\chi| \equiv \frac{|\omega_2|}{|\omega_1|} = \frac{1}{4} \qquad (27c)$$

locates the Lifshitz point L along a line of second-order transitions (T_c).

Consider now the expansion of the second derivative F" (the function Φ) in powers of the difference $q = h-h^o$ between the Miller index at some wave vector k in the axial direction and its value h^o at the appropriate special point:

$$\Phi = \Phi_o + \Phi_2\, q^2 + \Phi_4\, q^4 + \Phi_6\, q^6 + \ldots \qquad (28)$$

In Eq. (28), odd derivatives do not appear since they must vanish by symmetry at special point k^o at which they are evaluated. The coefficients Φ_n in Eq.(28) can be obtained by taking derivatives of the cosines in Eq.(25) at integral or half-integral values of h:

$$\Phi_n(T,\kappa) = \frac{1}{n!}\left[\frac{\partial^n\Phi}{\partial h^n}\right]_{k^o} \qquad (n=0,2,4,6,..)$$

yielding, in the clustering case,

$$\Phi_2 = 2\pi^2\,(\omega_1 + 4\omega_2)$$

$$\Phi_4 = -(2/3)\pi^4(\omega_1 + 16\omega_2)$$

and in the ordering case,

$$\Phi_2 = 2\pi^2(-\omega_1 + 4\omega_2)$$

$$\Phi_4 = -(2/3)\pi^4(-\omega_1 + 16\omega_2).$$

Hence, we have, for both cases,

$$\Phi_2 \geq 0 \quad \text{for} \quad |\chi| \leq 1/4$$

and

$$\Phi_4 \geq 0 \quad \text{for} \quad |\chi| \geq 1/16 .$$

It is thus seen that the coefficient Φ_4 must be always positive whenever the condition for the existence of long-period modulations

$$|\chi| \geq 1/4 \quad ,$$

obtained from Eqs.(27a) and (27b), is satisfied.

This is contrary to the conclusion reached by Aslanyan and Levanyuk *[34]* who claimed that a negative Φ_4 coefficient was more likely than a positive one. These author's conclusion is based on the consideration of first-neighbor pair interactions only, and therefore cannot apply to modulated structures. Only the introduction of pair interaction of greater range than the second axial neighbor, or the presence of anomalous entropy effects, could possibly reconcile a negative Φ_4 with the condition for the existence of modulations.

Since the coefficient Φ_4 was shown, in all likelyhood, to be positive for the model considered here, then, as in the usual Landau theory, it is sufficient to terminate the expansion (28) at the fourth-order term. We now seek the optimal wave vector which minimizes the function Φ at arbitrary point T, κ, i.e., we must find $q^* = h^*-h^o$ which minimizes

$$\Phi = \Phi_o + \Phi_2 q^2 + \Phi_4 q^4 . \tag{29}$$

Setting the derivative equal to zero yields two values

$$q^* = 0 \tag{30a}$$

and

$$q^* = \pm \sqrt{-\Phi_2/2\Phi_4} \quad , \tag{30b}$$

the second solution being valid for $\Phi_2 < 0$. Inserting Eq.(30) into (29) gives

$$\Phi_{min}(T,\kappa) = \begin{cases} \Phi_o & \text{for} \quad \Phi_2 > 0 \qquad (31a) \\ \Phi_o - \frac{1}{4}\frac{\Phi_2{}^2}{\Phi_4} & \text{for} \quad \Phi_2 < 0. \qquad (31b) \end{cases}$$

Note that setting Φ_{min} equal to zero in Eq.(31b) is equivalent to

$$\Phi_2{}^2 - 4\Phi_o\Phi_4 = 0, \tag{31c}$$

which is the condition for the polynomial (29) to have a double zero of value $q = 0$.

Both branches of Φ_{min} join smoothly at $\Phi_2 = 0$, so that, in accordance with the Lifshitz point definition, point L must have coordinates (T_L, κ_L) determined by the conditions

$$\Phi_o(T_L,\kappa_L) = \Phi_2(T_L,\kappa_L) = 0. \tag{32}$$

The line of second-order transitions in the (T,κ) plane is thus given by

$$\Phi_{min}(T,\kappa) = 0 \tag{33}$$

since, by Eqs.(23) and (24), it is the locus of the topmost (highest-temperature) vanishing of the coefficient F" of the second-order term in the Landau expansion. The locus $\Phi_{min} = 0$ is shown as a heavy dashed line in the schematic diagram of Fig. 4, drawn for the case of both J_1 and $J_2 < 0$. The Lifshitz point L is located at the intersection of this line and that which represents the vanishing of Φ_2. In a mean-field (BW) treatment of the ANNNI model, the value of κ_2 would be 1/4, as explained above. To the "left" of κ_L, the disordered phase (D) will transform

continuously to the ordered phase O_1, of SP ordering wave vector $k^*=k^o$; to the right, the disordered phase will transform continuously to a modulated phase (Mod) of non-SP wave vector $k^*\neq k^o$. The value of q^*, Eq.(30), will increase continuously from its value zero as the parameter κ increases from its limit value κ_L.

The locus of $\Phi_o=0$ to the "right" of κ_L is also indicated in Fig. 4 (light dashed line). It is clear that the latter line must lie below the T_c line ($\Phi_{min}=0$), so that $\Phi_o=0$ must represent a "special-point instability" or ordering spinodal *[28,29]* below which the amplitude of the appropriate (clustering or ordering) SP wave can grow spontaneously if, perhaps for kinetic reasons, the modulated phase were prevented from developing. Signs of the functions Φ_{min}, Φ_o and Φ_2 in various regions are also shown in Fig. 4, in that order.

Figure 5a illustrates the behaviour of the second derivative F" centered about a special point; the full curve represents the function Φ of Eq. (25) with $|\omega_2|/|\omega_2| = 0.45$, and the dashed curve is its Taylor's expansion, Eq. (28), taken to 4th order only. Figure 5b indicates schematically the behaviour of the function Φ at points on the (T,κ) plane at corresponding points in Fig. 4.

Figure 6 illustrates the formation of "domains" by a harmonic wave of half-period M= 98/19 = 5.1579 , a typical value for CuAu II periodic antiphase structures (see Sect. 5). The modulating function f(x), of amplitude A can be written

$$f(x_p) = A \cos 2\pi h^* p = A \cos 2\pi(h^o+q)p$$

$$= A[\cos 2\pi qp \cos 2\pi h^o p - \sin 2\pi qp \sin 2\pi h^o p]$$

where p is a space coordinate which takes on integer values at all lattice plane positions. Since, at these positions, the sine terms in the expansion

of the cosine must vanish according to Eq. (26a), the modulating function can equivalently be considered as a cosine ordering wave of index h^o (full curve in Fig. 6) amplitude-modulated by a long-period wave of index q, i.e. of (half) wavelength M (dotted curve). The effect on the lattice of this amplitude-modulated wave is exactly the same as that of the original $f(x_p)$, the latter shown as a dotted curve in Fig.6.

The transition between O_1 and Mod phases can be first or second-order, depending upon the relative symmetries of the phases. The transition line is the locus of equality of F^* and F^o evaluated at the wave vectors which minimize the free energies in modulated and O_1 phases, respectively. If the transition is second-order then, by continuity, the optimal wave vector <u>at</u> the transition must be k^o itself, so that the line of critical temperatures between O_1 and Mod regions must coincide with the line $\Phi_2=0$ (dot-dash curve in Figure 4). If the transition is first-order, the locus of equality of free energies (full line) must lie in the negative Φ_2 region, but must meet the $\Phi_{min}=0$ at the Lifshitz point where the transition becomes second-order.

The case $\Phi_4>0$, just described, was initially treated by Hornreich, et al.*[25,26]*, but already anticipated by Haas *[35]*; the case $\Phi_4<0$, $\Phi_6>0$ was first proposed by Aslanyan and Levanyuk *[34]*. Both cases were summarized by Toledano *[36]*, including that of expansions of Φ containing odd powers of q. However, because the present authors consider the case $\Phi_4<0$ to be highly unlikely, it will not be treated here. Instead, the low-temperature expansion of the exact free energy of the ANNNI model about the multiphase point κ_o will now be summarized.

4.2 Multiphase Point

The low-temperature expansion of the ANNNI model's exact free energy was performed about multiphase point κ_o by Fisher and Selke (FS) *[14]*. Let us summarize here the FS method and results. The model treated by these authors is the one depicted in Fig. 7: atoms on a tetragonal lattice interact via in-plane (square lattice) effective pair interactions J_o, and via first (J_1) and second-neighbor (J_2) pair interactions along the four-fold rotational symmetry axis.

The free energy is

$$F = - k_B T \ln Z \tag{34}$$

where the configurational partition function is expressed as

$$Z = \sum e^{-E(\sigma)/k_B T} \tag{35}$$

in which the configurational energy for this model is given by

$$E = - \frac{1}{2} \sum_p \sum_r \sum_\rho [J_o \, \sigma(p,r)\sigma(p,r+\rho)$$

$$+ J_1 \, \sigma(p,r)\sigma(p\pm 1,r) + J_2 \, \sigma(p,r)\sigma(p\pm 2,r)], \tag{36}$$

for exactly equiatomic concentration of A,B atoms (no applied magnetic field, in the language of magnetism).

In Eq.(35), the summation is over all possible states of energy $E(\sigma)$, with σ designating any configuration defined by assigning to the "site occupation operator" the values:

$$\sigma(p,r) = \begin{cases} +1 \text{ if atom A is at site } (p,r) \\ -1 \text{ if atom B is at site } (p,r) \end{cases}$$

to each lattice site at position r in lattice plane p normal to the axial direction. The summations in Eq.(36) are over all positions r in all planes p, and, in given layer p, over first neighbors ρ of points r.

Thus far, the treatment is exact, but of course the summation in Eq.(35) cannot be carried out. At very low temperatures, there are only a few "wrong" site occupancies, however, so that configurations which contribute significantly to the free energy F are very few, and can be enumerated explicitly. The problem treated by FS was the clustering (ferromagnetic) case, for which both J_0 and J_1 interactions are positive. In order for long-period structures to develop, the interaction J_2 must "compete" with J_1, i.e. create frustration, hence J_2 must be negative (antiferromagnetic). With these assignments for the choice of signs of J_0, J_1, J_2, FS were able to predict the existence of long-period polytypes of structure type $\langle 2^j 3 \rangle$, according to the notation described in Sect. 3.2. These authors also derived a phase diagram showing regions of stability of such phases in the vicinity of a multiphase point found to be located at $T=0^oK$ and $\kappa_0=|J_2|/J_1=1/2$.

A simple transformation allows the application of FS results to the ordering (antiferromagnetic) case, characterized by J_0, J_1, J_2, all negative, as was shown elsewhere *[37]*. Let us summarize those results here. A simple square lattice with negative (antiferromagnetic) nearest-neighbor interactions possesses a ground state in which each site has four nearest neighbors with the opposite value of σ so that there are no "wrong bonds." The results of FS can then be directly applied to this case

in the following manner. First, notice that each lattice site in a simple tetragonal structure can be labeled as "even" or "odd" such that each even (odd) site has four in-layer nearest neighbors and two axial nearest neighbors which are all odd (even). Now, changing the signs of J_0 and J_1 is equivalent to a transformation in which all the signs of the σ variables on odd (or even) sites are reversed. To see this, consider the configurational energy given by Eq. (36). In the nearest neighbor summation, the products of σ variables always appear in even-odd pairs, while in the axial next-nearest neighbor summation, pairs are always even-even or odd-odd combinations. Thus, in a given configuragion, a transformation that reverses all σ's at the odd (or even) sites while simultaneously changing the signs of J_0 and J_1 leaves the configurational energy (36) invariant. The conclusion is that the equilibrium configurations, for the case J_0, J_1, $J_2<0$ are obtained from those for the case $J_0, J_1>0$, $J_2<0$ simply by reversing the signs of σ (A, B occupation) on all odd (or even) sites.

Figure 8 is a schematic drawing of the phase diagram in the κ-T plane for the case $J_0, J_1, J_2<0$. This diagram is really the same as that derived by FS *[14]*, being obtained by applying the aforementioned transformation to all the phases predicted by FS. An example of this transformation applied to a one-dimensional chain is illustrated in Fig. 9 showing how a structure $\langle 2^j 3\rangle$ is transformed to $\langle 2^{j+1} 1\rangle$. An example of the $\langle 2\ 1\rangle$ phase on the full three-dimensional lattice is shown in Fig. 10, inspired from that given in Ref. *[38]*.

4.3. Schematic Phase Diagram

It is instructive to combine, in a qualitative manner, the results of expansions at both Lifshitz and Multiphase points into a global phase diagram incorporating, wherever possible, information gained from mean field *[11]* and Monte Carlo studies *[13]*. Only the *zero-field case* (vanishing magnetic field or difference of chemical potentials) will be treated. The resulting schematic phase diagram shown in Fig. 11 is believed to be a plausible one, even though the nature of the long-period phases, which now populate the "Mod" region shown previously in Fig. 1, is not known with certainty. It will be argued here that all of these phases must be "Fujiwara-type", i.e. must have structures derived from the continued fraction algorithm described in Sect. 3.2.

The case $J_1<0$, $J_2<0$, $J_n(n\geq 3)=0$ was chosen for illustration, hence the long-period phases must be $\{2^j1\}$ polytypes, as indicated in Fig. 11. The Lifshitz point L has been placed near its BW value of 1/4, and the $D\rightarrow O_1$ and D→Mod transitions (in the notation of Fig. 1) have been assumed to be second-order. Consequently, at and just below T_c, to the "right" of L (κ increasing), quasi-sinusoidal ordering waves of infinitesimal amplitude are expected to become stable, with wave vector index h^* given by Eq. (26b). Since all possible values of h^* (or q^*) are *a priori* equally probable, an infinity of incommensurate phases are expected. In fact, incommensurate modulations will dominate the phase diagram in those temperature ranges since *[15]*, from a strictly mathematical viewpoint, the set of rational numbers p/q has measure zero in the field of real numbers.

As the temperature in the Mod region is decreased, the modulation

wave amplitude will increase, and the profile will sharpen, approaching that of a square wave. Although Monte Carlo simulations have shown *[13]* that the third harmonic of the modulation function f(x) tends to persist to temperatures close to T_c, no evidence has been found for even harmonics, thereby supporting our contention that only square-wave, or FW phases can be present in an equilibrium phase diagram of this sort. At lower temperatures, both increase in amplitude and "squaring" of profile will enhance the tendency of the modulations to "lock in" at commensurate wavelenths (in the sense of the definition given in Sect. 2) with relatively small commensuration number P. Hence, well below T_c, phase regions of "simple" FW polytypes will tend to broaden, or bulge out, thereby practically squeezing out incommensurate phase fields. This bulging out is particularly noticeable in the <21> phase region; it is already apparent in the curvature of the <21>:<221> boundary in Fig. 8, calculated by the low-temperature expansion, and is demonstrated in mean-field calculations *[11]*.

As long as the lock-in tendency is weak, the modulation wavelength will tend to vary almost continuously with temperature, at given value of κ, the correct q^* being obtained by minimizing the free energy in k-space. Monte Carlo studies *[13]* indicate that, close to T_c, the average wavelength appears to vary continuously with T (or κ). In these simulations, wavelength increase is observed to take place by means of a mechanism similar to the one that has been described elsewhere, in another context *[39]*, as a "local doubling of the period". The actual modulated structure will appear to be rather irregular; indeed, two-dimensional MC simulation *[40]* shows quite clearly that the boundaries between domains have the "wavy" appearence described in Sect.3.3. Such "non-rigid soliton walls" (in

the words of Bak and von Boehm *[11]*) are associated with high configurational entropy, and are thus favored at high temperature.

At lower temperatures, wavy boundaries cost too much internal energy, so that planar domain walls should be the rule below a certain "interface roughening transition". It is not known at present whether this transition is sharp or gradual, although three-dimensional Monte Carlo studies *[13]* indicate a rather sharp one, as does a much earlier model of Inglesfield's *[42]* which treats antiphase boundary motions as a two-dimensional Ising model. Below this transition, sharp or diffuse, the modulation period should vary discontinuously, jumping as it were from one commensurate phase to the next. As the temperature is further reduced, the ANNNI model predicts the complete disappearence of long-period phases, leaving only the ordered phases denoted O_1 and O_2 in Fig. 1, or <1> and <2> in the particular example illustrated in Fig. 11.

The conjecture that all polytypes in the ANNNI model must be FW phases was stated above. Clearly, the low-temperature expansion predicts FS phases, which form a subset of FW phases. Recently, Duxbury and Selke *[42]* have shown, by mean-field calculations, that polytypes whose structure formulas are combinations of FS units ($<2^j3>$ in this instance) appeared in the phase diagram through a "structure combination branching mechanism", i.e. the boundary between two FS phases, such as <23> and $<2^23>$ splits to produce a $<232^23>$ phase, which then gives rise to $<(23)^22^23>$, etc.. These authors have demonstrated the stability of polytypes which belong to the set of FW phases, whose structural formulas are derived by the continued fraction algorithm described in Sect.3.2, and shown in Apendix I to correspond to a square wave modulation.

In Fig. 11, we have attempted to show schematically this branching

mechanism, producing FW phases of increasing complexity, i.e. of increasing level of continued fraction expansion. Only phases of level 1 and 2, selected from Table II, have been indicated in Fig. 11. Around and in between the illustrated phase fields will presumably be found infinitely many long-period structures of infinitely increasing commensuration number P, with infinitely decreasing field extent, separated by phase boundaries of progressively decreasing first-order character. Because of the very small free energy difference between neighboring high-level polytypes, it will be very difficult to calculate the domains of existence of these phases and very difficult to observe them experimentally.

Note that, because of the bulging of the central <21> phase field at fixed κ just greater than 1/2, the long-period wavelenth will tend to decrease as the temperature decreases in the higher temperature range, close to T_c, whilst the opposite effect should be obseved in the temperature ranges just below the bulge. At large values of κ, however, the ANNNI model predicts that the modulation wavelength should inrease monotonically with decreasing temperature. All of those conclusions should be reversed for <23>-type phases.

Such are some of the predictions of the simple ANNNI model. Let us now see whether these results can be applied to real ordered alloy systems.

5. APPLICATION TO FCC ORDERING

Two well studied alloy systems have antiphase structures which are strikingly similar to those of the polytypes described above: the electronically similar Au_3Zn and Ag_3Mg ordered phases at and slightly off stoichiometry. The former belongs to the $\langle 2^j3 \rangle$ type, the latter to the $\langle 2^j1 \rangle$ type. Structures $\langle 2^33 \rangle$ and $\langle 2^41 \rangle$ are shown in Figs. 12a and 12b, as determined by high-resolution transmission electron microscopy by Van Tendeloo and Amelinckx *[43]* and by Portier *et al.* *[38]*, respectively. Formally, the correspondence between Figs. 12 and 10 can be accomplished by subdividing the (disordered phase) fcc lattice into two tetragonal sublattices, one occupied by alternating Au (Ag) and Zn (Mg) atoms, the other by noble metal atoms only. If one ignores the pure noble metal sub-lattice one obtains exactly the structures illustrated in Fig. 10, depicting FS phases predicted by the low-temperature expansion of the ANNNI model. One must of course assume that the true fcc near-neighbor interactions in these systems produce the correct ground-state structures, the <u>axial</u> interactions J_1 and J_2 then being considered as superimposed <u>effective</u> pair interactions responsible for the long-period modulations. These arguments can be made more rigorous, as explained in Appendix II.

The DO_{23} ground state, $\langle 2 \rangle$ in the FS notation, has been observed in both Au_3Zn and Ag_3Mg, and FS phases $\langle 2^j1 \rangle$, with j=2,3,4, and 6 have been reported in Ag_3Mg *[38]*. FS phases $\langle 2^33 \rangle$ and $\langle 3 \rangle$ have been seen in Au_3Zn *[43]*. There is as yet no unambiguous evidence of higher-level FW phases, although Portier *et al.* have published a Ag_3Mg high-resolution micrograph (Fig. 7 of Ref. *[38]*) with both $\langle 2^41 \rangle$ and $\langle 2^31 \rangle$ polytypes present. The

authors concluded that the microstructure presented "stacking disorder". In fact, the micrograph in question shows no "faults", and the whole structure could be described as $\langle 2^4 1(2^4 1 2^3 1)^m \rangle$, with integer m unknown because the imaging field was not large enough to cover the whole period. The polytype structure just given can be easily proved to be a FW phase, an example of which, with m=4, was given in Table I (Q=41).

These experimental findings can be interpreted in the light of the ANNNI model in the following way: let J_1 and J_2 be *effective axial* pair interactions; then, J_1 must be positive for Au_3Zn, negative for Ag_3Mg, and J_2 must be negative for both. The value of κ must be greater than 1/2 since the ground state must be the DO_{23} structure, represented by <2>. Furthermore, the in-plane interaction J_0 must be negative to produce two-dimensional ordering in the planes normal to the axial direction, and the absolute value of this parameter is expected to be relatively large since antiphase boundaries remain straight in the temperature ranges investigated. Available evidence *[44]* indicates that the average domain size M increases with increasing temperature in Ag_3Mg, thus suggesting that the measurements were performed in the temperature region above the <21> bulge in the ANNNI phase diagram, with values of κ just greater than 1/2.

The interpretations just given must be taken with some caution, however, as phase equilibria in actual alloy systems may differ appreciably from those deduced from the simple ANNNI model. Furthermore, the $D \rightarrow O_1$, or D→Mod transitions may well turn out to be first-order, if they could be brought about experimentally. Nevertheless, the analogy between the observed Ag_3Mg polytype structures and the FS predictions is really striking. This can be seen most dramatically in Fig. 13, a very high-resolution TEM micrograph gratiously provided to the present authors

by Drs. N. Kuwano and T. Eguchi *[45]*. In this figure, the bright spots represent the positions of projected columns of Mg atoms, the Ag atoms being out of contrast. The periodic antiphase shifts of double and single lines of Mg atoms clearly indicate a $\langle 2^3 1 \rangle$ structure.

Historically, the best-known long-period superstructures are those of the Cu-Au system. In the phase field traditionally labeled CuAu II, close to the equiatomic composition, the average modultion half-period has value M of about 5. Recent TEM work *[22]* has shown clearly that the antiphase boundaries have a "wavy" appearance, unlike the very straight ones of Au_3Zn or Ag_3Mg. To interpret these observations in the light of the ANNNI model, it is necessary to postulate long-range <u>effective</u> pair interactions at least out to fourth <u>axial</u> neighbor. It is indeed shown in Appendix III that, with $J_1>0$ and $J_4<0$, and all other pair interactions small in magnitude, the ground state for $\kappa'=-J_4/J_1>1/4$ should be given by $\langle 4 \rangle$, and the central "bulging" phase should have structure formula $\langle 5 \rangle$. The ground state for $\kappa'<1/4$ is then $\langle \infty \rangle$, as in the original SF calculation, which, with $J_0<0$, represents the simple $L1_0$ ordered structure, i.e. CuAu I. A phase diagram much like the one of Fig. 11 should then result, but with phase fields appropriately relabeled, as indicated schematically in Fig. 14. Near-stoichiometric CuAu could then be modeled with a κ' value somewhat smaller than its value at the multiphase point κ_0. The fact that antiphase boundaries experimentally are found to be wavy would indicate that the range of stability of the "Mod" phases lies above the postulated interface roughening transition.

An interesting effect was observed on CuAu by Guymont and co-workers *[22]*: a stoichiometric alloy quenched directly from high temperature into the CuAu II phase field produced the $\langle 5 \rangle$ structure with M

exactly equal to 5. However, the same alloy held for a long time just above the CuAu II transition temperature produced, upon subsequent aging in the CuAu II phase field, a periodic antiphase structure with M slighly larger than 5. The authors interpreted these results in terms of "easy long-period fluctuations" assumed to exist just above the ordering temperature. We suggest an alternative interpretation based on the diagram of Fig. 14: for the indicated value of κ', the <5> phase field is seen to be preceded in temperature by a narrow Mod region which must contain closely spaced quasi-incommensurate FW phases with practically continuously varying modulation period. A direct quench from the disordered phase D into <5> would produce the expected average period of M=5, but the intermediate aging treatment in the incommensurate phase field would result in a stable FW phase with $M \neq 5$. Because of the very small differences in free energies, the resulting incommensurate structure could well remain in metastable equilibrium after continued aging in the CuAu II phase field proper. If the transition from D→Mod(incomm.) were second-order, it would be very difficult indeed to distinguish experimentally the incommensurate stable phase field from a solid solution phase field with "easy long-period fluctuations".

The characteristic difference between Ag_3Mg-type and CuAu-type long period superstructures has led Guymont and Gratias *[19]* to propose the following empirical rule: *those periodic antiphase structures which display straight domain walls have long-period strucures (polytypes) which persist to low temperatures, those which display wavy boundaries have long period structures which disappear at low temperatures.* We would prefer to regard both types of structures as two different manifestations of the same ANNNI-like behaviour: the "straight" systems would correspond to κ values

to the "right" of the multiphase point, the "wavy" systems to κ values to the "left" of that point. The fact that, in the former case, antiphase boundaries appear straight may simply be due to the experimental impossibility of getting close to the disordering temperature, thus precluding preparation of an ordered phase above the interface (antiphase domain wall) roughening transition. That long-period phases persist to low temperatures in the "straight" case may be explained by the very small difference between the free energy of FW phases and that of the <2> phase, itself having a (relatively) long period. By contrast, the disordering temperature is readily accessible in the CuAu case, with Mod phase fields lying above the roughening transition, as already mentioned. To confirm the validity of this interpretation, it would be necessary to discover a system for which the inerface roughening transition could actually be followed experimentally.

6. DISCUSSION

The main theme developed here is that, with the ANNNI model, we finally have a promising framework for coming to grips with the enigma of long-period superstructures. This is not to say that older theories, such as those of Sato and Toth (ST) and later modifications are thereby supplanted; certainly not: the ANNNI model treatment has nothing to say about the physical origin of the effective pair interactions J_1 and J_2, so that, ultimately, an electronic theory will be required to justify, for example, the value of κ used to model a given alloy system. What was lacking in earlier treatments, of course, was the all-important statistical mechanical aspect. Not that gallant efforts had not been made to incorporate thermodynamics into previous models; but all these attempts had relied on *mean field*, actually *Bragg-Williams* (BW) theories. Not surprisingly then, essential aspects of long-period behaviour could not be explained, such as: the variation of modulation wavelength with temperature at constant interaction parameters, the tendency for the modulation to lock in at small "commensuration numbers", the disappearence of long period superstructures at low temperatures, the "straight to wavy" transition, and the very nature of the structural polytypes themselves. True, the mathematical difficulties encountered in solving even the simplest ANNNI model has, so far, precluded a completely satisfactory resolution of the difficulties, but at least, as we have attempted to show, a general coherent picture is beginning to emerge.

Recall that a low-temperature expansion of the exact free energy (FS) has predicted unambiguously the existence of $\langle X_o^j Y_o \rangle$ polytypes (with

X_o, Y_o differing by one integer). Although a formal thermodynamical proof is still lacking, there are good indications *[42]* that the more general polytypes $\langle X^j Y \rangle$ [with X and Y representing nested FS stacking sequences, as determined by the continued fraction algorithm] will be the actual equilibrium phases. Exact treatments of the one-dimensional ANNNI chain *[33]* have also shown how, at fixed κ, the SRO modulation wavelength varies continuously with temperature, from its predicted BW value to that given by the exact ground state analysis. If electronic theories (such as that of ST) were to yield reliable estimates of, say, J_1 and J_2, then Eq. (26b), with J's substituted for ω's, would predict the modulation wavelength reliably. Thus, paradoxically, the original ST theory, though actually derived for zero temperature, is expected to do well only at high temperatures. As the temperature is lowered, the ω's in Eq. (26b) are no longer equal to the J's, and more accurate statistical models than the BW are essential for precise determination of the modulation wavelength.

Hence, the average modulation (half) wavelength M is determined by a combination of factors: the ratio J_2/J_1, the configurational entropy correction to the J's, the lock-in to simple polytypes. If the mathematics were tractable, it would then be possible to compute theoretically a model phase diagram such as that of Fig. 11, with no guesswork. It is important to emphasize that, *if* the ANNNI Hamiltonian represents the essential physics of the problem, then an exact statistical thermodynamical theory, or at least a reliable approximate formulation thereof, will yield all the desired features: the structural formulas of stable polytypes and their phase fields, the nature (first or second-order) of the transitions, and the character of the antiphase boundaries, straight, wavy, sharp or diffuse. Of course, the simple ANNNI Hamiltonian may not be adequate to

model an actual alloy system; it may well be necessary to include more elaborate schemes of effective interaction parameters, including long-range elastic forces. The resulting phase diagram may then be substantially modified, but not, we beleive, in an essential way.

The formal connection between the ANNNI model and the square wave modulation idea (Fujiwara phases) has not been made yet, but we are quite confident that a more detailed mathematical analysis of the model will confirm our conjecture about the structure of stable polytypes to be found in the phase diagram. It may appear unlikely that a phase such as $<2^{37}1>$, say, should be stabilized by relatively short-range forces only: how does the system "know" that after 37 double-plane domains the 38th one should be single-plane? Actually, the system needs to be "aware" only of the modulation wavelength M=P/Q, a value which, as just mentioned, is fixed by effective pair interactions whose range is of the order of M. The polytype structure itself is determined geometrically by the square wave modulation: it is as if the antiphase boundaries, at fixed M, interacted with one another through convex repulsive potentials. The commensuration number (75 in the above example) results simply from a sort of *Vernier* effect.

The continued fraction algorithm provides a criterion for determining whether a given stacking sequence of ordered lattice planes, observed by high resolution electron microscopy, represents an equilibrium phase or an "intergrowth": it suffices to count the number of lattice planes (P) in the period and to divide by the corresponding number of domains (Q). The ratio M must then be expanded in continued fraction as in Eq. (14) and the structural formula <X> of Eq. (18) compared to the observed stacking sequence. If there is perfect match, then the obseved microstructure is that of a single equilibrium polytype, otherwise not.

7. SUMMARY

The most important points made in this paper are the following:

An operational definition of *commensurate* and *incommensurate* modulations was proposed (Sect. 2).

The name *Fujiwara phases* was proposed to designate the polytypes conjectured to be found in the ANNNI model phase diagram. It was demonstrated that these "FW phases" resulted from a modulation of the lattice by a periodic function having only odd harmonics in its Fourier spectrum, for example a square wave.

Structural formulas for Fujiwara phases were shown to result from the continued fraction expansion of the modulation (half) period (Appx. I).

The most likely assignment of signs in the Lifshitz point expansion of the ANNNI model was discussed (Sect. 4.1).

The low temperature expansion of the exact free energy of the ANNNI model was summarised (Sect. 4.2), and the original result of Fisher and Selke was extended to the case of ordering on an fcc lattice (Appx. II).

A schematic ANNNI model phase diagram was proposed based on the results of published calculations (Sect. 4.3).

It was shown qualitatively how the characteristics of both Ag_3Mg-type and CuAu II-type periodic antiphase structures could be understood in terms of the ANNNI model. The respectively "straight" and "wavy" nature of the antiphase boundaries for those two types of systems were argued to represent but two aspects of the same phenomenon: in the

former case, the observed structures must be formed below an *interface roughening transition*, in the latter case, above.

It was shown how a different scheme of effective axial pair interactions could lead to longer range average modulation periods, such as those encountered in the CuAu II long-period superstructures (Appx. III).

APPENDIX I

The proof that the continued fraction algorithm described in Sect. 3.2 generates the correct square wave modulation polytypes (or FW phases) rests on the approximation of a rational fraction P/Q by its successive *approximants* P_i/Q_i, obtained by truncating the continued fraction expansion at levels $i = 0,1,\ldots,k$. These approximants are given by the formulas:

$$P_o = n_o \quad , \quad Q_o = 1 \tag{A1,a}$$

$$P_1 = n_1 n_o + \gamma_o \ , \quad Q_1 = n_1 \tag{A1,b}$$

$$P_i = n_i P_{i-1} + \gamma_{i-1} P_{i-2} \tag{A1,c}$$

$$(i = 2,3,\ldots,k)$$

$$Q_i = n_i Q_{i-1} + \gamma_{i-1} Q_{i-2} \tag{A1,d}$$

with

$$P_k/Q_k = P/Q = M.$$

At the lowest level (level 0), the best approximation for M is clearly P_o/Q_o with $Q_o = 1$ and $P_o = n_o = X_o$. The "domain" of X_o identical layers comes closest to fitting in one half-period M of modulating square wave. The next best approximation of M by identical layers is then $Y_o = n_o + \gamma_o$ ($\gamma_o = \pm 1$). Hence, X_o will be called the *majority domain* and Y_o the *minority domain* at this level.

The next approximation (level 1) consists of fitting a composite domain into a multiple of half-periods M: instead of using only a single sequence of identical layers, one tries a mixture of majority and minority domains according to the formula

$$\langle X_1 \rangle = X_o^{j}\, Y_o^{j'}, \tag{A2}$$

so that exactly P_1 (+ and -) layers fit into exactly Q_1 square wave half-periods. We must then have, by Eqs. (A1,a) and (A1,b),

$$P_1 = jX_o + j'Y_o = n_1X_o + \gamma_o$$

and

$$Q_1 = j + j' = n_1.$$

The only possible solution is then

$$j = n_1 - 1 \quad \text{and} \quad j' = 1 \tag{A3}$$

Hence, formula (17,c) is proved for level 1, along with formulas (17,a) and (17,b).

If the continued fraction expansion for M does not terminate at level 1, which is the level of all FS phases, one proceeds to level 2 by using as building blocks X_1 and Y_1, the latter, consisting of just one more or one less X_o domain than X_1, clearly being the minority domain appropriate for level 1. Let P_1' be the commensuration number for Y_1, i.e. the number of layers contained in domain Y_1, and Q_1' the corresponding number of square wave half-periods in Y_1. By following the same line of reasoning that was used for level 1, one can show by direct computation that the polytype structure at level 2 is $\langle X_2\rangle = (X_1)^j(Y_1)^{j'}$ with $j = n_2-1$ and $j' = 1$.

Let us now prove that the procedure is correct at arbitrary level i, assuming it to be correct at the previous level i-1. We must have

$$P_i = jP_{i-1} + j'P'_{i-1} = n_iP_{i-1} + \gamma_{i-1}\, P_{i-2} \tag{A4,a}$$

and

$$Q_i = jQ_{i-1} + j'Q'_{i-1} = n_iQ_{i-1} + \gamma_{i-1}\, Q_{i-2} \tag{A4,b}$$

in which P_i, P_{i-1} and P_{i-2} are the commensuration numbers of $\langle X_i\rangle$, $\langle X_{i-1}\rangle$, and $\langle X_{i-2}\rangle$, respectively, with P'_{i-1} and P'_{i-2} the corresponding ones for $\langle Y_{i-1}\rangle$ and $\langle Y_{i-2}\rangle$. The Q's are defined similarly for the number of square

wave half-periods at the indicated levels. By using results assumed to be correct at level i-1, it can then be shown that both Eq. (A4,a) and (A4,b) are satisfied by $j = n_i - 1$ and $j' = 1$. Since Eqs. (A4) are two linear equations in two unknowns, the solution is unique. Hence, by induction, the algorithm defined by Eqs. (14) to (17) has been shown to be correct at all levels, including the terminal one $\langle X \rangle = X_k$, which is Eq. (18). At each level, the X_i domains fit exactly in the approximant $M_i = P_i/Q_i$, and the sequence terminates at $i = k$. This completes the proof.

As an example, take $M = 73/46$. Repeated use of Eq. (15) produces the following continued fraction

$$M = \frac{73}{46} = 2 - \cfrac{1}{2 + \cfrac{1}{2 + \cfrac{1}{3 - \cfrac{1}{3}}}} \cdots$$

The partial quotients are thus

i	n_i	γ_i
0	2	-1
1	2	+1
2	2	+1
3	3	-1
4	3	0

The successive approximants are

$$M_0 = \frac{P_0}{Q_0} = \frac{2}{1} = 2$$

$$M_1 = \frac{P_1}{Q_1} = \frac{3}{2} = 1.5$$

$$M_2 = \frac{P_2}{Q_2} = \frac{8}{5} = 1.6$$

$$M_3 = \frac{P_3}{Q_3} = \frac{27}{17} = 1.5882\ldots$$

$$M \equiv M_4 = \frac{P_4}{Q_4} = \frac{73}{46} = 1.5869...$$

The corresponding partial polytype structures are then

$$X_o = n_o = 2$$

$$Y_o = n_o + \gamma_o = 2-1 = 1$$

$$X_1 = 21$$

$$Y_1 = 2^2 1$$

$$X_2 = (21)(2^2 1)$$

$$Y_2 = (21)^2(2^2 1)$$

$$X_3 = (212^2 1)^2[(21)^2 2^2 1]$$

$$Y_3 = (212^2 1)[(21)^2 2^2 1]$$

$$\langle X \rangle = X_4 = [(212^2 1)^2(21)^2 2^2 1]^2[212^2 1(21)^2 2^2 1] \qquad (A5)$$

Note that direct application of Eq. (11) will give a structural formula identical to that derived from the continued fration algorithm only for particular choices of the shift parameter ϵ. For the natural choice $\epsilon = 0$, these two procedures will yield apparently different structures. However, because of translation symmetry, the structures are in fact equivalent, the continued fraction formula being built up from X^jY units with the majority domain X always leading off, the direct computation with $\epsilon = 0$ being built up from the same units, but with largest commensuration domain leading off. Hence, according to the latter method, inversions $X^jY \rightarrow YX^j$ may take place at any level. It is easy to show that such inversions, at any level i, say, merely cause a translation of the final structure by Y_i. This is because the explicit expansion of $\langle X \rangle$ into X_i and Y_i symbols always contains Y_i to the "power" one only. Hence, a sequence such as

$$....Y_i X_i^j Y_i....$$

can be written as either

$$....(Y_iX_i^j)Y_i... \quad \text{or} \quad ... \; Y_i(X_i^jY_i)....$$

In the above example, formula (11) with $\epsilon = 0$ would have given, instead of (A5):

$$\langle X \rangle = [(2^2121)^321]^2[(2^2121)^221],$$

as shown also on line "Q=46" in Table II. The latter equation can be derived from (A5) by the transformation

$$(21)(2^21) \rightarrow (2^21)(21)$$

$$(21)^2(2^21) \rightarrow (2^21)(21)^2,$$

equivalent to a translation by domain (21).

APPENDIX II

In this appendix we show how an ANNNI-type model might be applied to an A_3B ordered structure on an fcc lattice. To begin, consider a simple pair interaction model with interactions out to second nearest neighbors. The energy can be written

$$E = -\frac{1}{2}\sum_i \left[\sum_{\rho_0} J_0\, \sigma(i)\, \sigma(i+\rho_0) + \sum_{\rho_1} J_1\, \sigma(i)\, \sigma(i+\rho_1)\right] - \mu \sum_i \sigma(i),$$

where the σ's are defined in the text, i labels the lattice site, and μ is an external field (difference of chemical potential). The vectors ρ_0 are the set of twelve vectors connecting a site to its nearest neighbors at (1/2)<110>. The ρ_1 comprise the set of six vectors <100> connecting a site with its second nearest neighbors. Here, a represents the edge of the standard cube of the fcc lattice. We consider the case where $J_0<0$, $J_1>0$, and μ falls in the appropriate range to give an $L1_2$ structure.

Alloys that exhibit long periods are known in many cases to have flat regions of Fermi surface normal to the <110> directions, and these are expected to give rise to long range pair potentials. With this in mind, we introduce a third pair interaction into our model that will end up stabilizing a periodically antiphased structure. This interaction, characterized by a strength $J_2 = -\kappa J_1 < 0$, couples a given site with its twelve neighbors at the positions <220>. It is thus a relatively long range interaction, but such effective interactions are not unexpected when Fermi surface effects are involved.

The occurrence of a long period in one direction will break the cubic symmetry of the $L1_2$ structure. There is equal probability for the long

period to occur along any one of the three cubic axes. In this example, let us choose [100] as the direction of the long period. Then there are two types of planes normal to [100]: pure A planes and mixed A-B planes. Denote these planes as p and m respectively (see Fig. 15). Notice that eight of the twelve <110> directions have components along ±[100]. Thus, eight of the twelve J_2 couplings will play a role in stabilizing the long period. These eight interactions couple sites in planes which are two unit cells apart, so J_2 here plays essentially the same role as the interaction J_2 in the original ANNNI model.

We assume that the only effect of introducing J_2 is the possible occurrence of antiphase boundary planes normal to [100]. With this assumption we now determine the ground states.

We first note that there are several contributions to the ground state energy which remain unaffected by the presence of antiphase domains. These contributions are: 1) energy due to the external field μ; 2) energy of any atom in a p-plane; 3) energy due to first-neighbor couplings of an atom in an m-plane; 4) energy of an atom in an m-plane due to the four second neighbor interactions along [001],[00$\bar{1}$],[010], and [0$\bar{1}$0]; 5) energy of an atom in an m-plane due to the four J_2 couplings along [011],[01$\bar{1}$],[0$\bar{1}$1], and [0$\bar{1}\bar{1}$]. One can calculate the energy per atom ΔE from these contributions and one finds

$$\Delta E = -\frac{1}{2}\mu - J_1\left(\frac{5}{2} - 4\kappa\right) \qquad \text{(AII-1)}$$

The interesting contribution to the ground state energy comes from the two second neighbor interactions along ±[100] and from the eight J_2 coulings mentioned above. These are the competing interactions that

stabilize the long periods. We shall refer to this contribution to the energy as the "axial" part.

If we allow antiphasing, there are two possibilities for the configuration of an m-plane. These two possibilities are the same as those indicated on the tetragonal lattice of Fig. 10. As in that figure, we designate the two cases as α and β. Now, we adopt the definition given by FS of k-bands. A k-band is a sequence of k consecutive m-planes of the same type (i.e., no antiphasing) terminated at both ends by antiphased m-planes. From this point, we can apply the analysis of FS. There are no 1-bands (no domains of size one) just as FS showed for the original ANNNI model.

A particular m-plane or site in an m-plane can be characterized by its relationship (antiphased or not) with the neighboring m-planes. As in FS, we must consider the following five possibilities, where the overstrike denotes the plane or site in question.

o	$\alpha\alpha\bar{\alpha}\alpha\alpha$
π	$\alpha\alpha\bar{\alpha}\alpha\beta$
ρ	$\beta\alpha\bar{\alpha}\alpha\beta$
σ	$\alpha\alpha\bar{\alpha}\beta\beta$
τ	$\beta\alpha\bar{\alpha}\beta\beta$

The labels o,π,ρ,σ, and τ are the same as those used by FS. If we assume 2N atoms in the crystal, there will be N atoms in the m-planes. Then we can use the expressions obtained by FS for the numbers of the various types of sites. These are

$$N_O = N \sum_{k\geq 5} (k-4)\ell_k,$$

$$N_\pi = N \sum_{k\geq 4} 2\ell_k, \qquad N_\rho = N\ell_3 \qquad \text{(AII-2)}$$

$$N_\sigma = N \sum_{k\geq 3} 2\ell_k, \qquad N_T = 2N\ell_2.$$

Here, we have used the structural variables ℓ_k defined by

$$L_k = \ell_k L,$$

where L_k is the number of k-bands in a given configuration of the system, and L is the total number of m-planes (number of unit cubes along the [100] direction).

We also need the contribution to the axial energy from each of the five types of sites. These contributions will be essentially those calculated by FS but modified to take account of the multiplicity of the J_2 interactions. Defining $\kappa = 1/8 + \delta$, we have

$$\Delta E_O = -1/2\,(1-8\delta)J_1,$$

$$\Delta E_\pi = -J, \qquad \Delta E_\rho = -1/2\,(3+8\delta)J_1, \qquad \text{(AII-3)}$$

$$\Delta E_\sigma = 0, \qquad \Delta E_T = -1/2\,(1+8\delta)J_1.$$

Combining results (AII-1), (AII-2), and (AII-3) we find the ground state energy per atom:

$$E_O\{\ell_k\} = -\frac{1}{2}\mu - J_1(\frac{5}{2} - 4\delta) - 4J_1\delta[2\ell_2 + \ell_3 - \sum_{k\geq 5}(k-4)\ell_k].$$

The expression in square brackets is identical to that obtained by FS since the axial part of our model is essentially the same as the ANNNI model. Thus, for $\kappa<1/8$, the structure is $L1_2$ and for $\kappa>1/8$, the structure is DO_{23}. At $\kappa=1/8$, the ground state is infinitely degenerate.

We next perform a low temperature expansion to first order about the multiphase point at $T = 0$, $\kappa = 1/8$. That is, we examine the free energy at temperatures sufficiently low that, aside from the ground state, the major contribution to the partition function is from the first excited states, i.e. states in which one A (or B) atom is replaced by a B (or A) atom. We define the following expansion parameters:

$$w_\mu = e^{-2\mu/k_BT}\ , \quad w_o = e^{2J_o/k_BT}\ , \quad x = e^{-2J_1/k_BT}\ .$$

For the first excited states, the Boltzmann factors arising from J_o and μ are

$w_o^{-4}\, w_\mu$ for replacing A by B,

$w_o^{12}\, w_\mu^{-1}$ for replacing B by A.

The analysis is made simpler if one chooses $\mu = 8|J_o|$. This means that $w_o^{-4}\, w_\mu = w_o^{12}\, w_\mu^{-1} \equiv w$. This value of μ is within the range for an $L1_2$ structure. This choice of μ is not necessary, but it facilitates counting the excited states. With this value for μ, we can apply the first order results of FS almost directly. The reduced free energy to first order may be written

$$f\{\ell_k\} = \frac{-F_{2N}\{\ell_k\}}{2N\ k_B\ T} \approx \frac{-E_o}{k_BT} + \frac{\Delta Z_{2N}^{(1)}}{2N},$$

where $\Delta Z_{2N}^{(1)}$ represents the contribution from the first excited states. This quantity is described in FS and the reader is referred to these authors for details. Our reduced free energy is

$$f = -4\ K_o + \frac{1}{2} w x^{\frac{11}{2} - 4\delta} + \frac{5}{2} K_1 - \frac{8}{3} K_1 \delta + \frac{1}{6} w x^{\frac{7}{2} - 4\delta} (2 + x^{3+8\delta})$$

$$+ a_2(\delta)\ell_2 + \sum_{k\geq 4} a_k(\delta)\ k\ \ell_k$$

where, to leading order,

$$a_2(\delta) = \frac{8}{3} K_1 \delta - \frac{2}{6} wx^{\frac{7}{2}-4\delta} (2 - 3x^{1+8\delta} + x^{3+8\delta})$$

and, for $k \geq 4$,

$$k\, a_k(\delta) = -\frac{8}{3} K_1 \delta(k-3) - \frac{1}{2} wx^{\frac{7}{2}-4\delta} [\frac{2}{3}(k-3) - (k-4)x^{1-8\delta}$$

$$- 2x^2 + \frac{1}{3} kx^{3+8\delta}],$$

where $K_o = J_o/k_BT$ and $K_1 = J_1/k_BT$.

The previous three expressions are the same in all important respects to the analagous ones derived by FS. We thus conclude that there are at least three regions of stable phases originating at $T = 0$, $K = 1/8$: (a) an $L1_2$ structure, (b) a structure with antiphase domains of size 3, that is, a (3,3) antiphase or <3> state, and (c) a DO_{23} or <2> structure. The phase boundaries at low T should then look like those in Figure 1. The boundary between $L1_2$ and <3> is a true phase boundary at low enough temperatures, but the <3>-<2> boundary may be unstable in higher order with respect to the occurrence of more complex polytypes consisting of domains of size 2 and 3.

We note that if J_1 is sufficiently negative to stabilize a DO_{22} structure for $J_2 = 0$, then a finite $J_2<0$ will stabilize a <21> phase in the region near $\kappa = 1/8$. The <2> phase will again be stable for sufficently large κ.

APPENDIX III

We present here a low temperature expansion to first order of the model mentioned in Sect. 5; this is a simple modification of that discussed in Sect. 4.2, where we replace J_2 by J_4, i.e., we consider a pair interaction out to the fourth axial neighbor. We neglect any interactions between second and third axial neighbors. The configurational energy for this model is given by Eq.(36) if we make the replacement $J_2 \to J_4$ and $\sigma(p\pm2,r) \to \sigma(p\pm4,r)$. We choose $J_0<0$, $J_1<0$, and $J_4<0$.

At low temperatures, individual layers will be ordered such that each A atom has four B atoms as nearest neighbors and vice versa. The two possibilities for a given plane are denoted α and β as in Appendix II. The configuration of the entire system at low temperatures is then described by specifying each plane as α or β. It is thus convenient to use the concept of k-bands described in Appendix II.

Determining the ground state is essentially a one dimensional problem. One can show, using a cluster method [46], that for $|J_4/J_1| \equiv \kappa < 1/4$, the ground state is $\langle\infty\rangle$ (no antiphase boundaries), while for $\kappa>1/4$, the structure $\langle 4\rangle$ has lowest energy. A 4-band is in fact the smallest band that will occur, even at the multiphase point $T=0$, $\kappa=1/4$. We shall perform a first-order low temperature expansion about this multiphase point following the analysis presented by FS.

To begin, we must express the energy in terms of the structural variables ℓ_k described in Appendix II. We first classify each plane (or site) by specifying its four neighboring planes on either side, keeping in mind that there will be no k-bands for $k<4$. As in Appendix II, we have the

following classifications:

1.	$\alpha\alpha\alpha\alpha\bar{\alpha}\alpha\alpha\alpha\alpha$	7.	$\beta\beta\alpha\alpha\bar{\alpha}\alpha\beta\beta\beta$
2.	$\alpha\alpha\alpha\alpha\bar{\alpha}\alpha\alpha\alpha\beta$	8.	$\beta\beta\alpha\alpha\bar{\alpha}\alpha\alpha\beta\beta$
3.	$\alpha\alpha\alpha\alpha\bar{\alpha}\alpha\alpha\beta\beta$	9.	$\beta\alpha\alpha\alpha\bar{\alpha}\alpha\beta\beta\beta$
4.	$\alpha\alpha\alpha\alpha\bar{\alpha}\alpha\beta\beta\beta$	10.	$\beta\alpha\alpha\alpha\bar{\alpha}\alpha\alpha\beta\beta$
5.	$\alpha\alpha\alpha\alpha\bar{\alpha}\beta\beta\beta\beta$	11.	$\beta\alpha\alpha\alpha\bar{\alpha}\alpha\alpha\alpha\beta$
6.	$\beta\alpha\alpha\alpha\bar{\alpha}\beta\beta\beta\beta$		

Following FS, we calculate the numbers of each of these types of site. We must also determine the energy of each type. Omitting the details, we give the result for the energy, defining $\kappa \equiv 1/4 + \delta$:

$$E_o\{\ell_k\} = -2J_o - (3/4)J_1\delta\,[1 - 4\sum_{k\geq 7}(k-6)\ell_k + 8\ell_4 + 4\ell_5].$$

We have used the identity $\sum_{k\geq 4} k\,\ell_k = 1$. For $T = 0$, minimization of E_o with respect to the ℓ_k is consistent with the result already cited that for $\kappa < 1/4$ ($\delta<0$) the system is in the $\langle\infty\rangle$ state and for $\kappa > 1/4$ ($\delta>0$), the system is in the $\langle 4\rangle$ state.

We next analyze the first excited states. The reduced free energy is

$$f\{\ell_k\} = \frac{-F_N\{\ell_k\}}{Nk_BT} = \frac{-E_o}{k_BT} + \frac{\Delta Z_N^{(1)}}{N} + O(w^6),$$

with the expansion parameter $w = \exp(2J_o/k_BT)$. The quantity $\Delta Z_N^{(1)}/N$ is the contribution to the partition function of the first excited states and is described more fully in FS. Again, we omit the details and cite the result. The second expansion parameter is $x = \exp(-2J_1/k_BT)$ and $K_i=J_i/k_BT$ for $i = 0, 1$. The reduced free energy is then:

$$f = 2K_0 + \frac{3}{4} K_1 + \frac{3}{5} K_1 \delta + \frac{1}{5} (2 + 3x^{\frac{5}{2}+2\delta})w^4$$

$$+ a_4(\delta)\, \ell_4 + \sum_{k\geq 6} k\, a_k(\delta)\, \ell_k,$$

where

$$a_4(\delta) = \frac{8}{5} K_1\delta - \frac{2}{5} w^4(4 - 5x^{\frac{1}{2}+2\delta} + x^{\frac{5}{2}+2\delta}),$$

$$6a_6(\delta) = \frac{7}{2} a_7(\delta) = \frac{8}{3} a_8(\delta),$$

and, for $k\geq 8$,

$$k\, a_k(\delta) = -\frac{8}{5} K_1\, \delta(k-5) + \frac{1}{5} w^4[2(5-k)+5(k-8)x^{\frac{3}{2}-2\delta}$$

$$+30x^2-3kx^{\frac{5}{2}+2\delta}].$$

This result is similar to that obtained by FS for the original ANNNI model and the arguments (appropriately modified) carry over. For δ on the order of w^4, we obtain two phase boundaries in the δ-T plane. The first is a boundary between <∞> and <5>, and its locus, $\delta_{-\infty}(T)$, is given by

$$K_1\delta_{-\infty}(T) = -\frac{1}{4} w^4(1-x^{\frac{1}{2}})^2[(1 + 2x^{\frac{1}{2}} + 3x) + \frac{3}{2} x^{\frac{3}{2}}]$$

$$+ O(w^6).$$

This boundary is stable in higher order as well. The second boundary is between <5> and <4>. Its locus, $\delta_1(T)$, is given by

$$K_1\delta_1(T) = \frac{1}{4}w^4(4 - 5x^{\frac{1}{2}} + x^{\frac{5}{2}}) + O(w^6).$$

We expect this boundary to be unstable in higher order with respect to the occurrence of longer polytypes consisting of antiphase domains of size 4 and 5.

We note that one can change the sign of J_1 and obtain the three phases <1>, <2111>, and <211> in place of <∞>, <5>, and <4> respectively. Such polytypes have been observed in Cu_3Al [47].

ACKNOWLEDGEMENTS

The authors benefited greatly from helpful conversations with Drs. T. Eguchi, S. Amelinckx, G. Van Tendeloo, W. Selke, P. Toledano, D. Gratias and A. Finel. In particular, the authors thank Professor Eguchi for permission to use the micrograph reproduced here in Figure 13, and are grateful to Dr. Selke for constructive criticism concerning an earlier version of this manuscript.

This work was supported by the Director, Office of Energy Research, Office of Basic Energy Sciences, Materials Sciences Division of the U.S. Department of Energy under Contract No. DE-AC03-76SF00098.

REFERENCES

1. H. Sato and R.S. Toth, *Phys. Rev.* **124**, 1833 (1961); **127**, 469 (1961).

2. M. Tachiki and K. Teramoto, *J, Phys. Chem. Solids* **27**, 335 (1966).

3. T. K. Vul and M. A. Krivoglaz, *Phys. Met. Metall.* **53**, 1 (1981).

4. H. Sato and R.S. Toth, in *Alloying Behaviour and Effects in Concentrated Solid Solutions*, T. B. Massalski, Ed., p.295, Gordon and Breach, N.Y. (1965).

5. B. L. Gyorffy and G. M. Stocks, *Phys. Rev. Letters* **50**, 374 (1983).

6. R.J. Elliott, *Phys. Rev.*, **124**, 346 (1961).

7. J. von Boehm and P. Bak, *Phys. Rev. Letters* **42**, 122 (1979).

8. M.E. Fisher and W. Selke, *Phys. Rev. Letters* **44**, 1502 (1980).

9. W. Selke in *Nato Advanced Study Institute on Modulated Structure Materials*, T. Tsakalakos, Ed., Maleme-Chania, Crete (1983).

10. J. Villain and M.B. Gordon, *J. Phys. C: Solid St. Physics* **13**, 3117 (1980).

11. P. Bak and J. von Boehm, *Phys. Rev. B*, **21**, 5297 (1980).

12. F. Axel and S. Aubry, *J. Phys. C: Solid St. Phys.* **14**, 5433 (1981).

13. W. Selke and M.E. Fisher, *Phys. Rev. B* **20**, 257 (1979).

14. M.E. Fisher and W. Selke, *Phil. Trans. R. Soc.* **302**, 1 (1981).

15. W. Selke (private communication).

16. P. Perio and M. Tournarie, *Acta Cryst.* **12**, 1032 (1959).

17. G. Jehanno and P. Perio, *J. Phys. (Paris)* **25**, 966 (1964).

18. K. Fujiwara, *J. Phys. Soc. Jpn.* **12**, 7 (1957).

19. M. Guymont and D. Gratias, *Acta Cryst.* **A35**, 181 (1979).

20. J. Hubbard, *Phys. Rev. B* **17**, 404 (1978).

21. V.L. Pokrovsky and G.V. Uimin, *J. Phys. C: Solid St. Physics* **11**, 3535 (1978).

22. M. Guymont, R. Portier and D. Gratias, *Acta Cryst.* **A36**, 792 (1980).

23. H. Jones, *J. Phys. C: Solid St. Phys* **2**, 760 (1969).

24. R. Portier and D. Gratias, *Cristallographie des Transitions de Phases*, Ecole d'Ete, Aussois (Sept. 1979).

25. R.M. Hornreich, M. Luban and S. Shtrikman, *Phys. Rev. Letters* **35**, 1678 (1975).

26. R.M. Hornreich, M. Luban and S. Shtrikman, *Phys. Rev. B* **19**, 3799 (1979).

27. L.D. Landau and E.M. Lifshitz, *Statistical Physics*, p.366, Addison-Wesley, Reading, Mass. (1958).

28. D. de Fontaine, *Acta Metall.* **23**, 553 (1975).

29. D. de Fontaine in *Solid State Physics* **34**, pp.73-274, H. Ehrenreich, F. Seitz and D. Turbull, Eds., Academic Press, N.Y. (1979).

30. J.M. Sanchez, D. Gratias and D. de Fontaine, *Acta Cryst.* **A38**, 214 (1982).

31. R. Kikuchi, *Phys. Rev. B*, **81**, 988 (1951).

32. J.M. Sanchez, *Physica* **111A**, 200 (1982).

33. D. Gratias (unpublished research at U.C. Berkeley).

34. T.A. Aslanyan and A.P. Levanyuk, *Sov Phys. Solid State* **20**, 466 (1978).

35. C. Haas, *Phys. Rev. A* **140**, 863 (1965).

36. P. Toledano, to be published in *Multicritical Phenomena*, L. Lynn, Editor (Geilo, 1983).

37. J. Kulik and D. de Fontaine, in *International Conference on Phase Transformations*, Maleme-Chania, Crete (1983).

38. R. Portier, D. Gratias, M. Guymont and W.M. Stobbs, *Acta Cryst.* **A36**, 190 (1980).

39. D. de Fontaine in *Ultrafine-Grain Metals*, Syracuse Univ. Press, pp. 93-131 (1970).

40. W. Selke and M.E. Fisher, *Z. Physik B* **40**, 71 (1980).

41. J.E. Inglesfield, *J. Phys. F: Metal Phys.* **2**, 68 (1972).

42. P.M. Duxbury and W. Selke *J. Phys. A*: **16**, L741 (1983).

43. G. Van Tendeloo and S. Amelinckx, *Phys. Stat. Sol.* **a43**, 553 (1977).

44. A. Gangulee and S.C. Moss, *J. Appl. Cryst.* **1**, 61 (1968).

45. N. Kuwano and T. Eguchi (private communication). Part of the miocrograph of Fig. 13 appeared in the Proceedings of the 7th International Conf. on High-Voltage Electron Microscopy, Aug. 1983, Berkeley, CA.

46. A. Finel (private communication).

47. N. Kuwano, H. Mishio, M. Toki, and T. Eguchi, *Phys. Stat. Sol. a* **65**, 341 (1981).

TABLE I

All Fujiwara phases with P = 73, such that 1.5 < M < 2.0

Q	M	Structure
48	1.5208	$<[2^2 1(21)^{10}]^2 21>$
47	1.5532	$<[2^2 1(21)^3]^4 21>$
46	1.5870	$<[(2^2 121)^3 21]^2[(2^2 121)^2 21]>$
45	1.6222	$<[(2^2 1)^2 21]^5 2^2 121>$
44	1.6591	$<(2^2 1)^{14} 21>$
43	1.6977	$<[2^3 1(2^2 1)^2]^4 2^2 1>$
42	1.7381	$<2^3 1[(2^3 1)^4 2^2 1]^2>$
41	1.7805	$<2^4 1(2^4 12^3 1)^4>$
40	1.825	$<2^5 1[(2^5 1)^2 2^4 1]^2>$
39	1.8718	$<(2^7 1)^4 2^6 1>$
38	1.9211	$<(2^{12} 1)^2 2^{11} 1>$
37	1.9730	$<2^{36} 1>$

TABLE II

All possible Fujiwara phases with $2 \leq P \leq 20$ and all possible Q's such that $1.5 \leq M = P/Q \leq 2$

M	P/Q	Level k	Structure
1.5	3/2	1	$\langle 21 \rangle$
1.5454	17/11	2	$\langle 2^2 1(21)^4 \rangle$
1.5555	14/9	2	$\langle 2^2 1(21)^3 \rangle$
1.5714	11/7	2	$\langle 2^2 1(21)^2 \rangle$
1.5833	19/12	3	$\langle (2^2 121)^2 21 \rangle$
1.6	8/5	2	$\langle 2^2 121 \rangle$
1.625	13/8	2	$\langle (2^2 1)^2 21 \rangle$
1.6363	18/11	2	$\langle (2^2 1)^3 21 \rangle$
1.6666	5/3	1	$\langle 2^2 1 \rangle$
1.7	17/10	2	$\langle 2^3 1(2^2 1)^2 \rangle$
1.7143	12/7	2	$\langle 2^3 12^2 1 \rangle$
1.7272	19/11	2	$\langle (2^3 1)^2 2^2 1 \rangle$
1.75	7/4	1	$\langle 2^3 1 \rangle$
1.7777	16/9	2	$\langle 2^4 12^3 1 \rangle$
1.8	9/5	1	$\langle 2^4 1 \rangle$
1.8333	11/6	1	$\langle 2^5 1 \rangle$
1.8571	13/7	1	$\langle 2^6 1 \rangle$
1.875	15/8	1	$\langle 2^7 1 \rangle$
1.8888	17/9	1	$\langle 2^8 1 \rangle$
1.9	19/10	1	$\langle 2^9 1 \rangle$
2.0	2/1	1	$\langle 2^\infty 1 \rangle = \langle 2 \rangle$

FIGURE CAPTIONS

Fig. 1. Schematic phase diagram indicating Disordered (D), Simple Ordered (O_1), Complex Ordered (O_2), and Modulated (Mod) pase regions. Lifshitz point at L, Multiphase point at κ_o. Coordinates are temperature T and interaction parameter ratio κ. Full curves represent first-order, dashed curves second-order transitions.

Fig. 2. Simulated diffraction patterns for long-period polytypes decribed in text. Sizes of filled circles indicate relative intensities. Open circles represent fundamental reflections at Miller index h = 0 and 1.

Fig. 3. Stacking of A and B-rich planes with antiphase shifts occurring approximately every five lattice spacings in the x direction. Bottom portion of figure indicates projected antiphasing modulation f(x), illustrating smooth profile corresponding to wavy antiphase boundary in upper potion of figure.

Fig. 4. T-κ Phase diagram in vicinity of Lifshitz point L. Loci of vanishing of various functions are indicated. Triplets of signs denote regions where functions Φ_{min}, Φ_o, and Φ_2, respectively, have the indicated signs. Behaviour of function Φ at temperatures T_a, T_b, T_c, T_d, (at κ_-) T_1, T_c, T_2, and T_3 (at κ_+) are shown in Fig. 5b.

Fig.5a. Second derivative function $\Phi(h)$ about point h=1/2 (ordering case), full curve, and its Taylor's expansion to 4th order, dashed curve; both plotted for κ = 0.45.

Fig.5b. Values of function Φ (Taylor's expansion) plotted *versus* modulating wave index q at values of κ (κ_+ and κ_+) and temperatures indicated in Fig. 4. Triplets of signs have same meaning as in Fig. 4.

Fig. 6. Antiphase domains formed by modulating wave $f(x_p)$, dotted curve. Effect of this wave on the lattice is the same as that of amplitude modulated ordering wave, full curve, whose envelope is the long-period modulation shown as dashed curve. Half-period of latter modulation is $M = 98/19 = 5.1579$.

Fig. 7. Tetragonal unit cell for ANNNI model, indicating lattice-site notation and effective pair interaction parameters J.

Fig. 8. ANNNI model phase diagram obtained by FS low-temperature expansion for "ordering" case: $J_1<0$ and $J_2<0$.

Fig. 9. Sign transformation procedure for deriving "ordering" from "clustering" phase diagram.

Fig.10. Antiphase structures $<2^41>$ (a) and $<2^33>$ (b) with associated tetragonal unit cell (top portion of figure).

Fig.11. Conjectured ANNNI model phase diagram, similar to diagram of Fig. 1 but with breakup of Mod phase field indicated schematically. Only a few FW phases are shown; infinitely many others are expected, for instance in regions covered by light dashed lines.

Fig.12. Periodic antiphase structures observed in fcc alloys: $<2^41>$ in Ag_3Mg (a) and $<2^33>$ in Au_3Zn (b). Note similarity with Figs. 10a and 10b, respectively.

Fig.13. High-resolution TEM micrograph taken by N. Kuwano using the JEM-1000 Microscope at the HVEM Laboratory of Kyushu University, Japan, of Ag_3Mg exhibiting long-period superstructure $<2^31>$. Light dots are projections of rows of Mg atoms, Ag atoms are not imaged.

Fig.14. Portion of ANNNI model phase diagram assumed to be appropriate to CuAu II-like systems. At indicated value of parameter κ', the long-period polytype phase field <5> is shown surmounted by a narrow phase field of "incommensurate" modulations produced from the disordered phase D by a second-order transition.

Fig.15. Two types of (100) planes in the $L1_2$ ordered structure: m planes present A-B ordering, p planes contain only one type of atom.

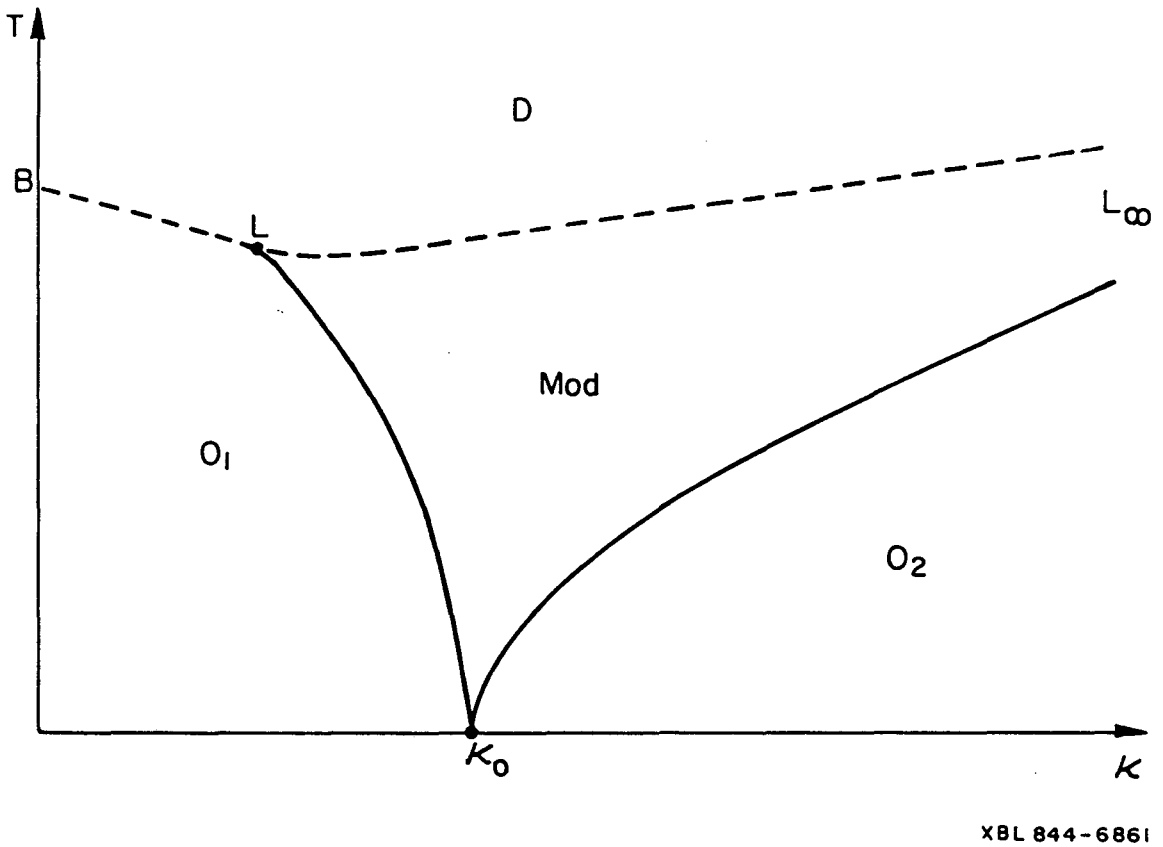

Figure 1.

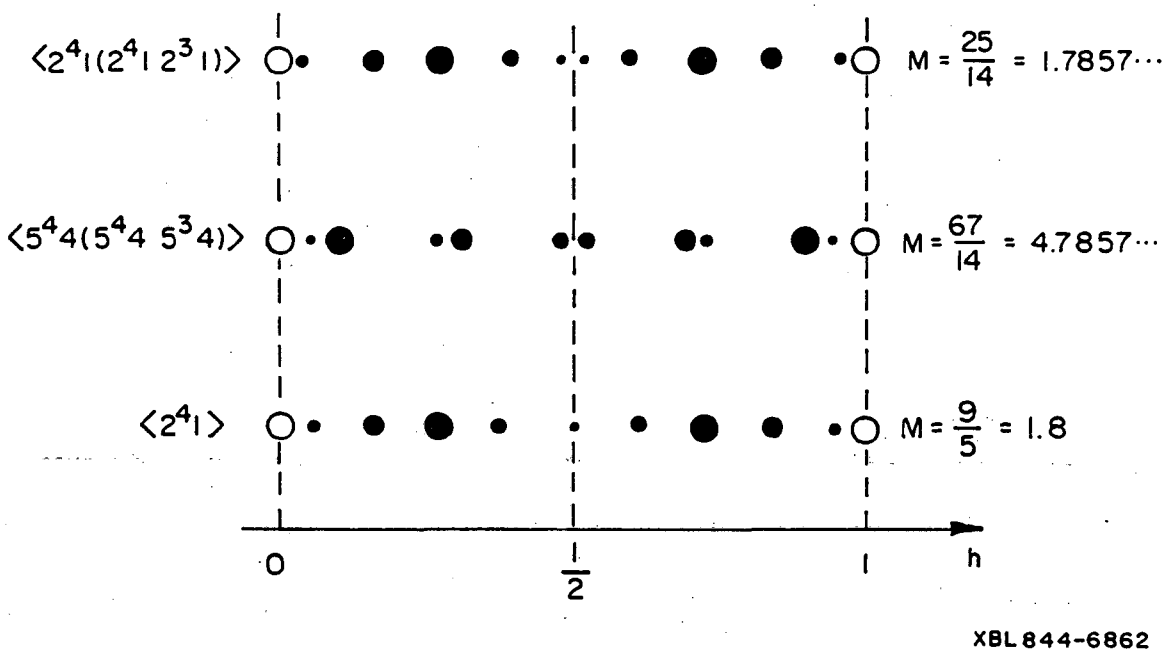
$\langle 2^4 1(2^4 1\, 2^3 1)\rangle$
$M = \frac{25}{14} = 1.7857\cdots$
$\langle 5^4 4(5^4 4\, 5^3 4)\rangle$
$M = \frac{67}{14} = 4.7857\cdots$
$\langle 2^4 1\rangle$
$M = \frac{9}{5} = 1.8$
0
$\frac{1}{2}$
1
h
XBL 844-6862

Figure 2.

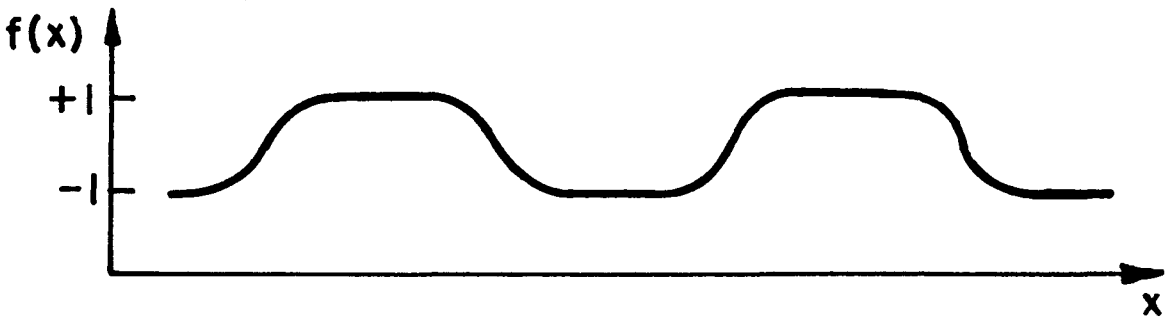

XBL 844-6863

Figure 3.

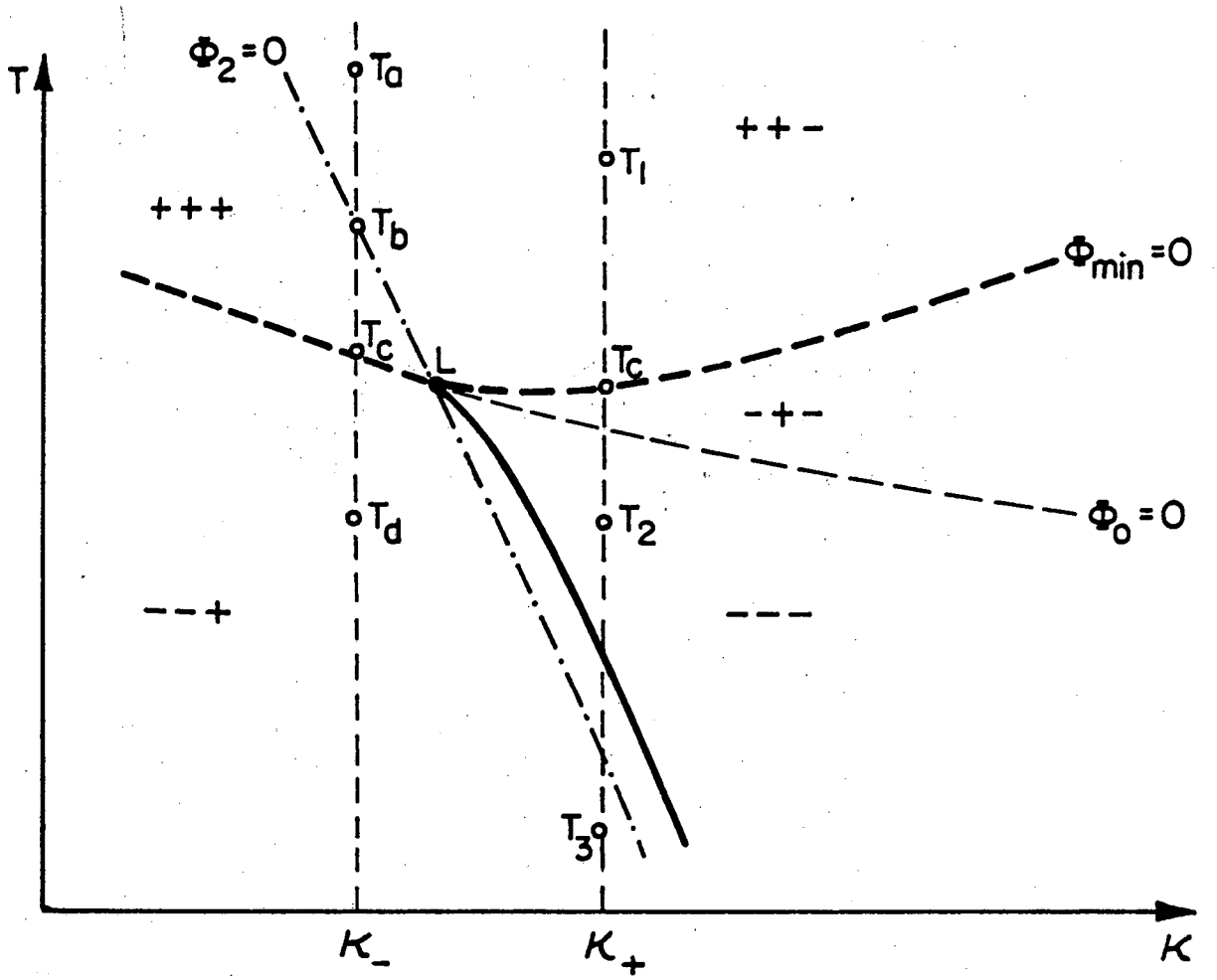

XBL 844-6864

Figure 4.

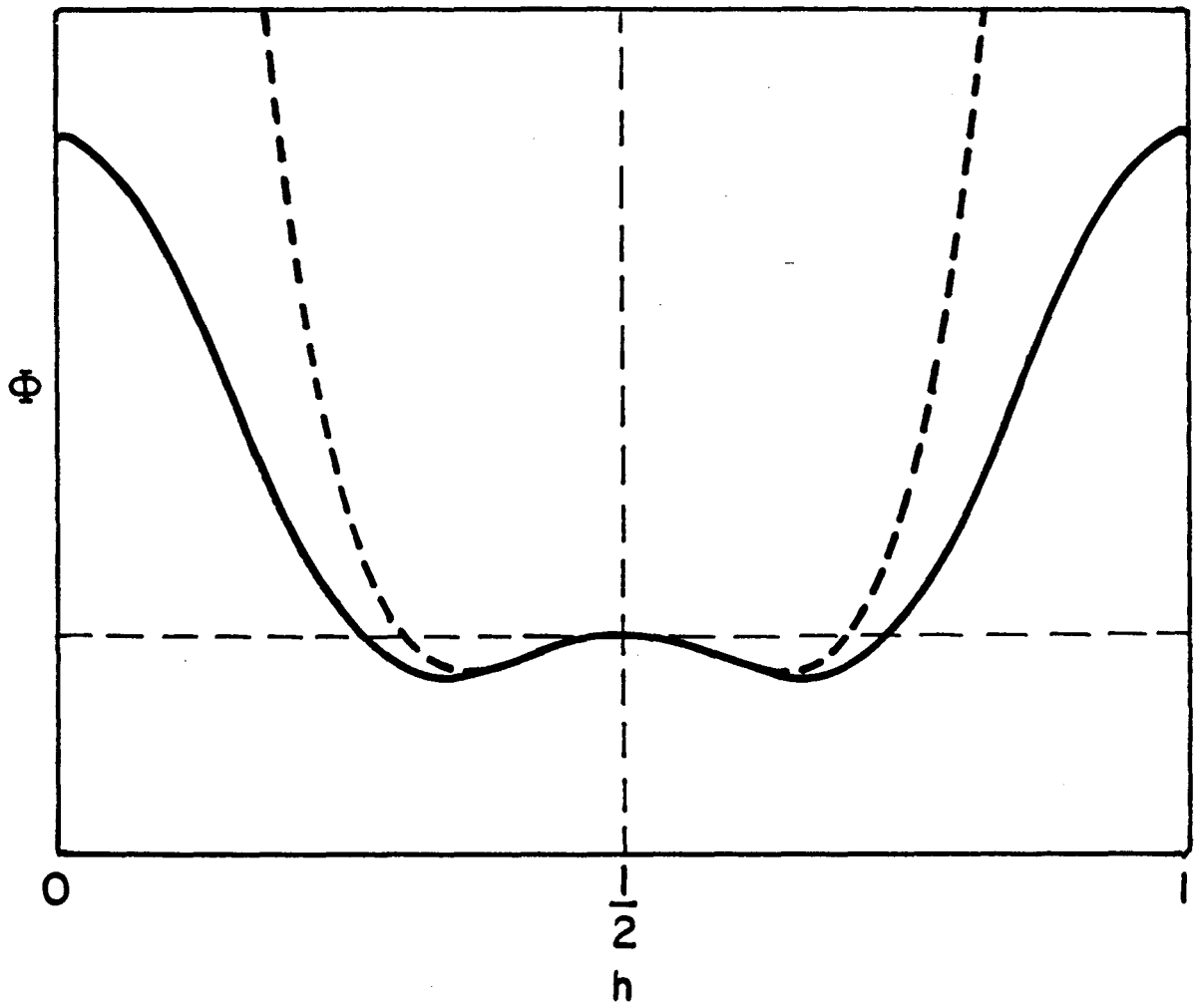

XBL 844-6865

Figure 5.

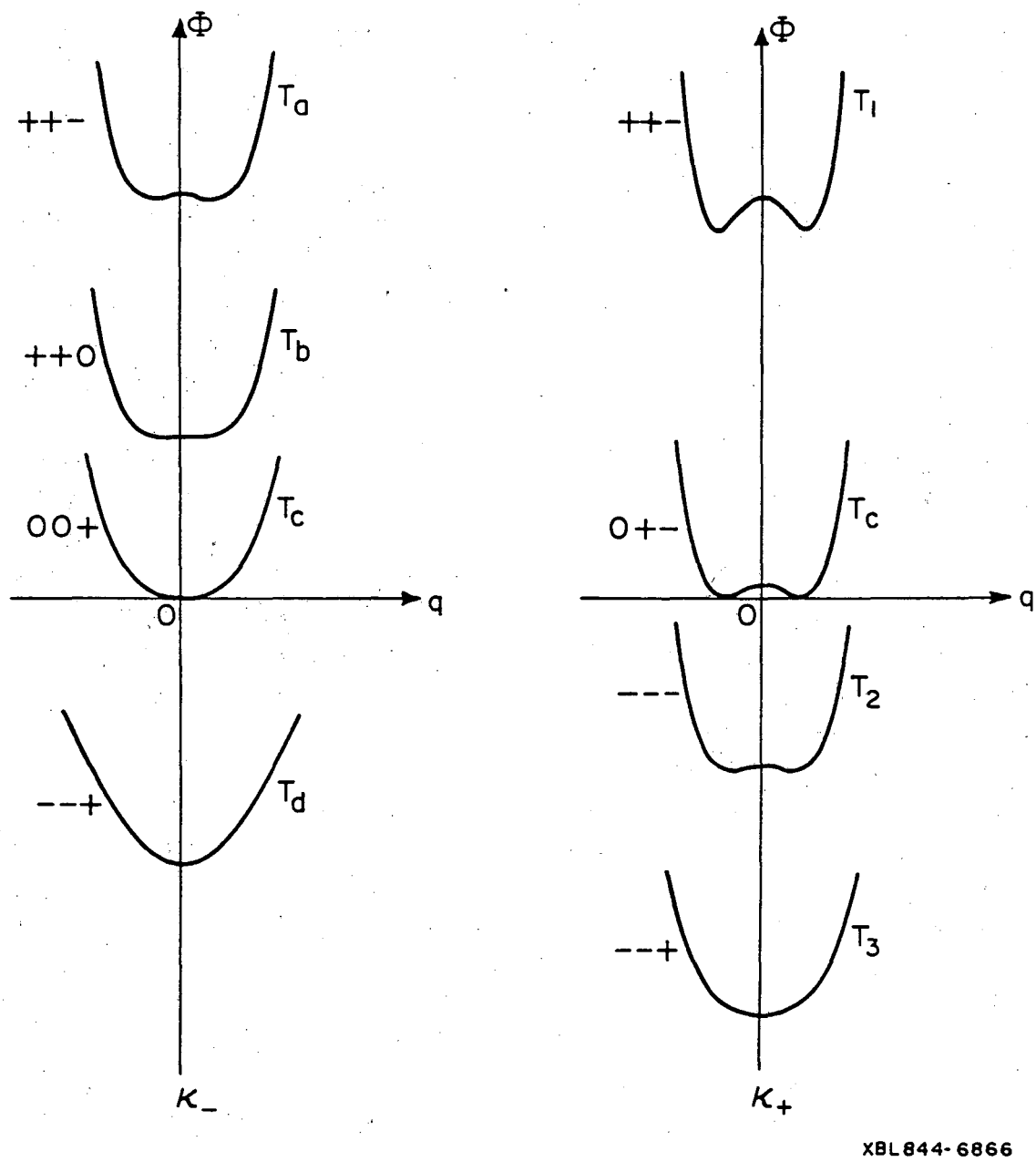

Figure 6.

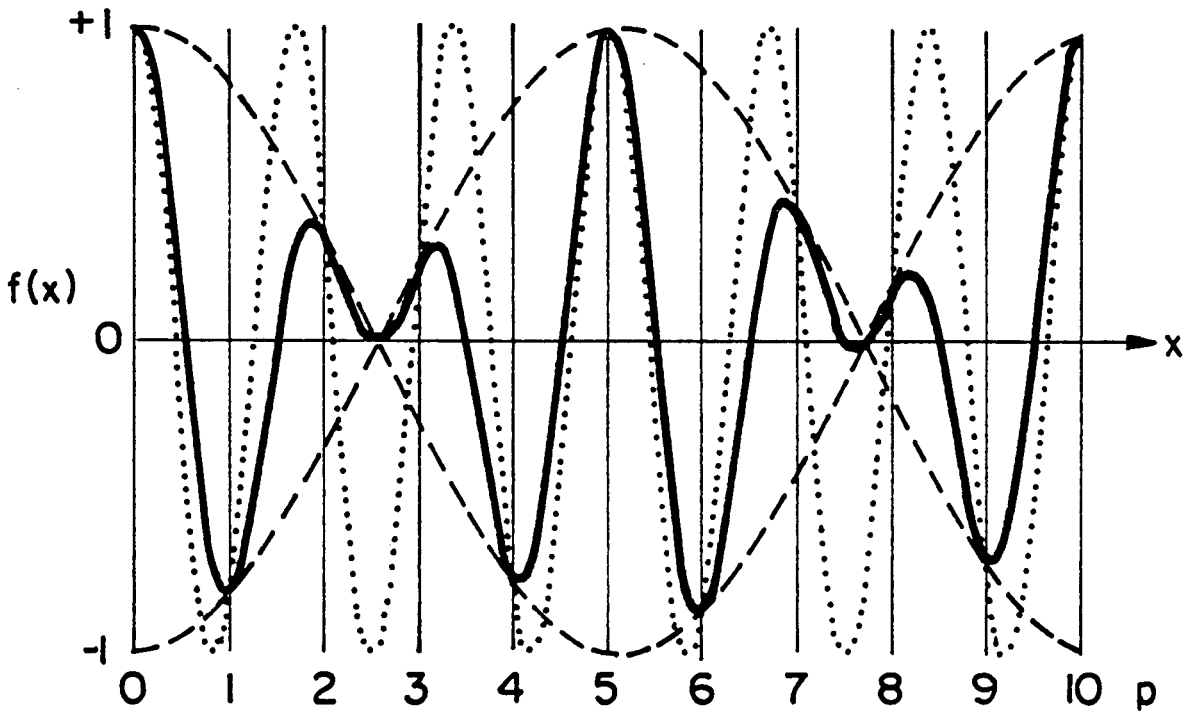

XBL 844-6867

Figure 7.

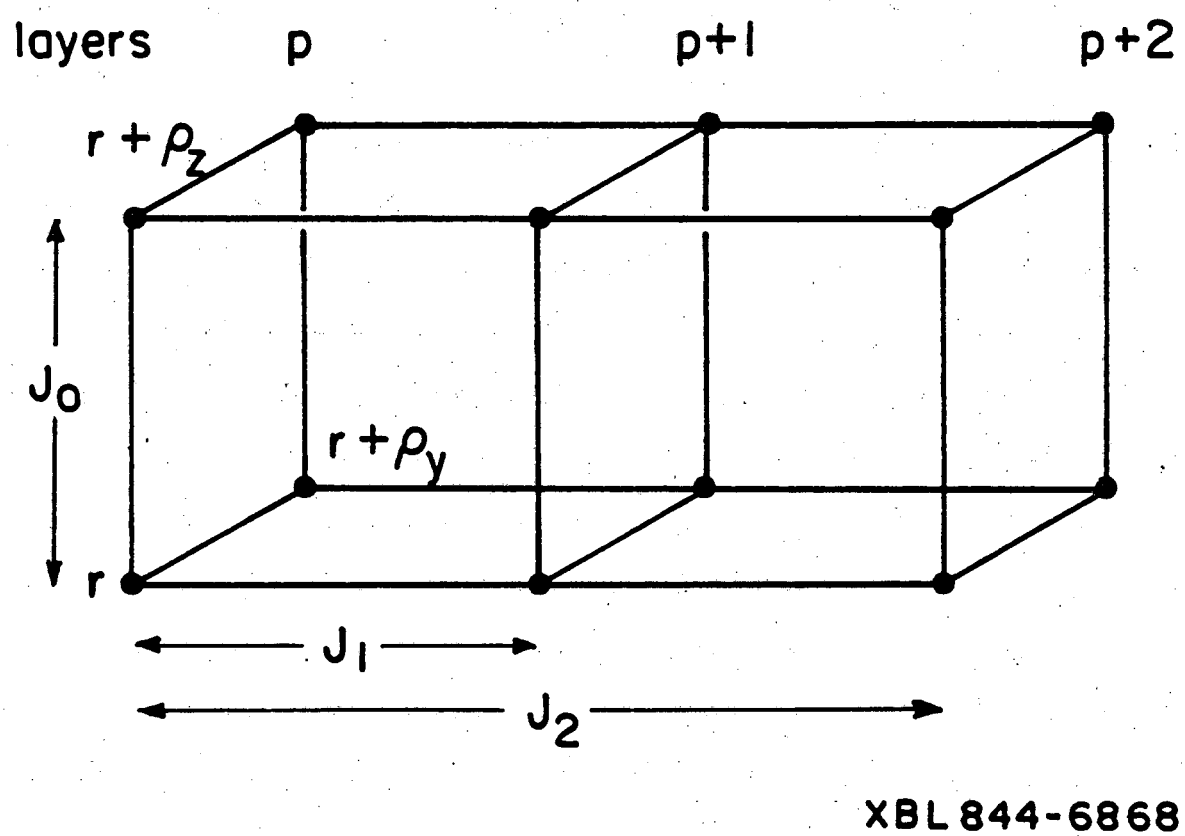

Figure 8.

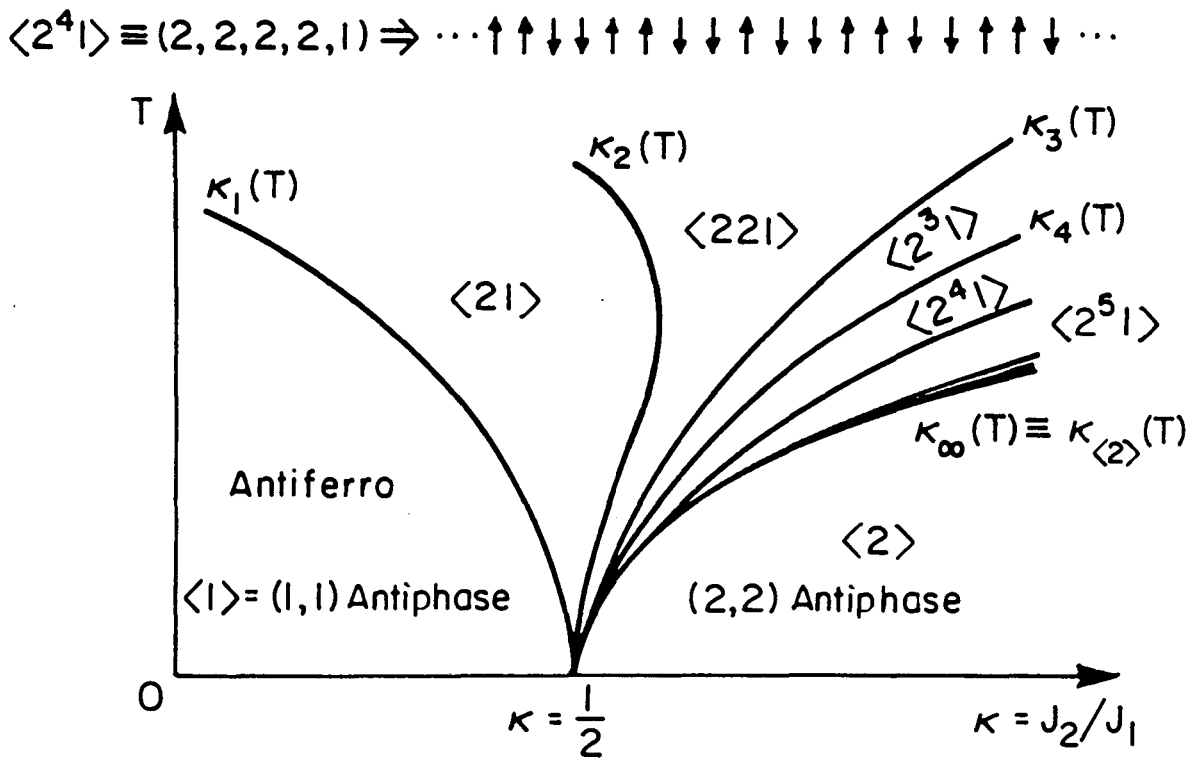

Figure 9.

XBL 835-5750

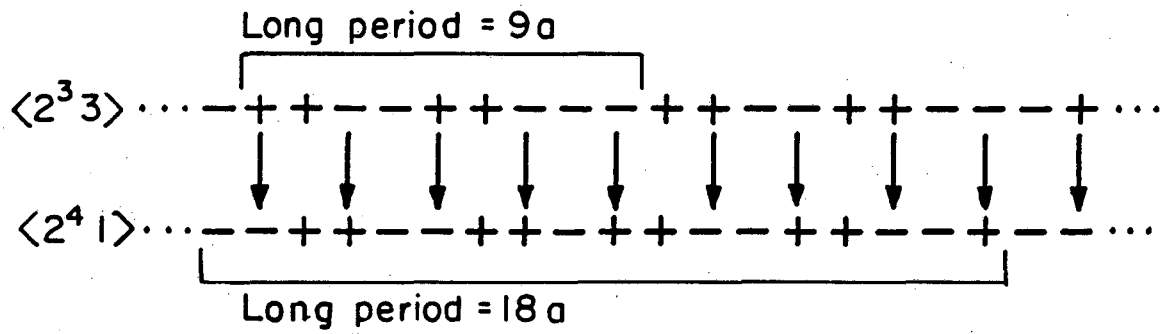

XBL 835-5751

Figure 10.

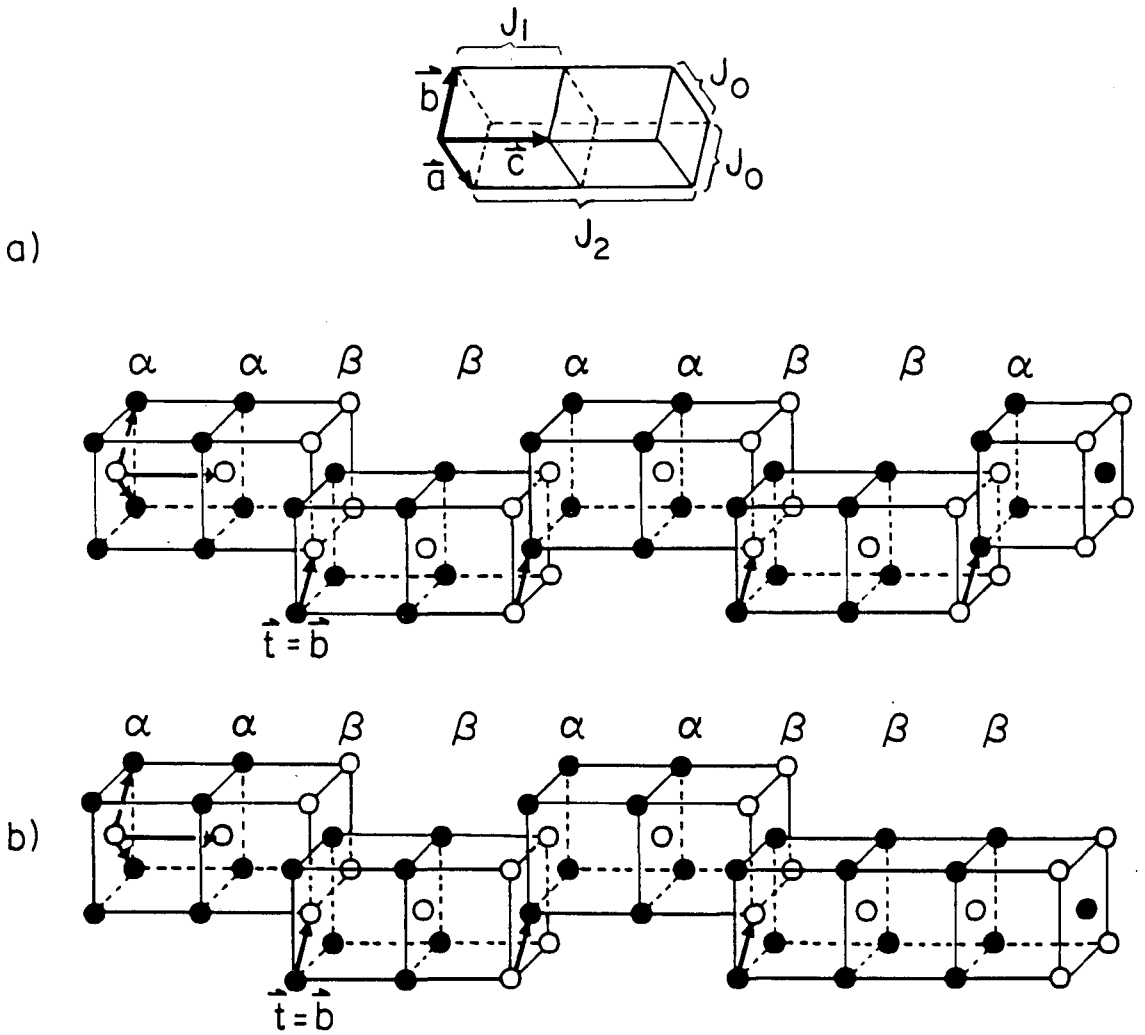

Figure 11.

XBL 835-5752

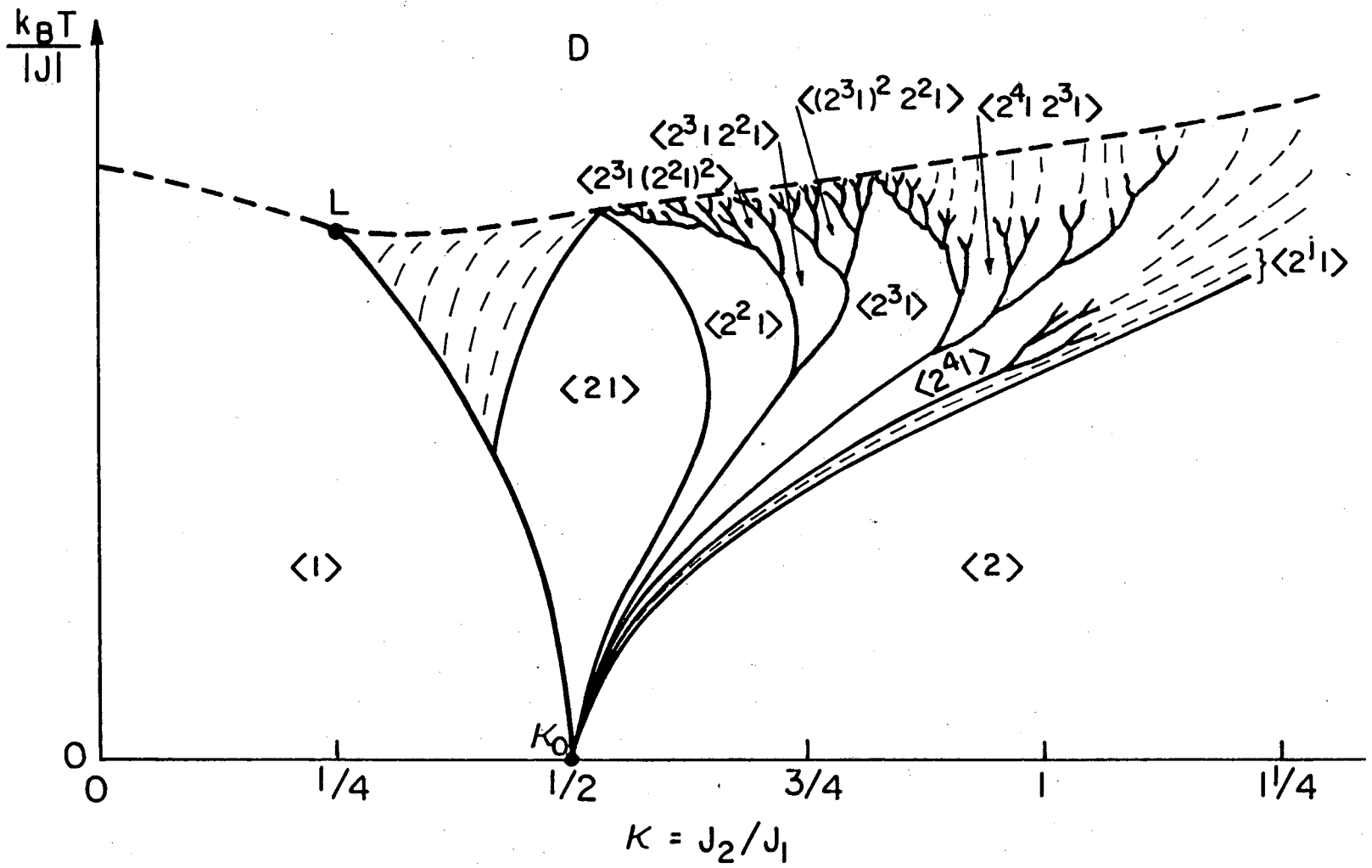

Figure 12.

XBL 844-6869

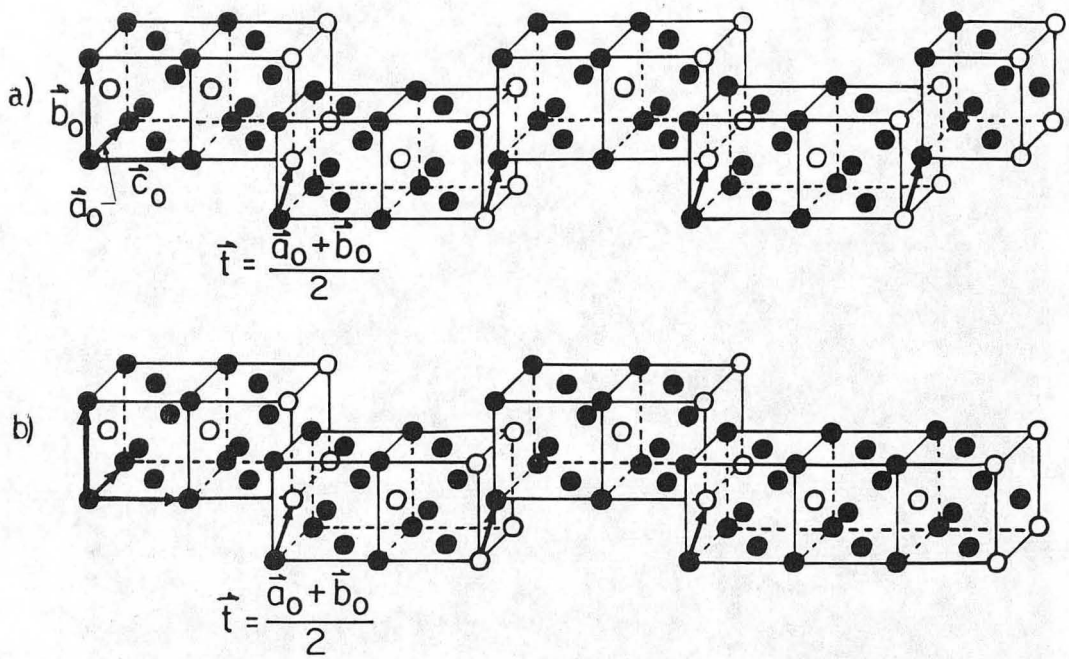

XBL 835-5752A

Figure 13.

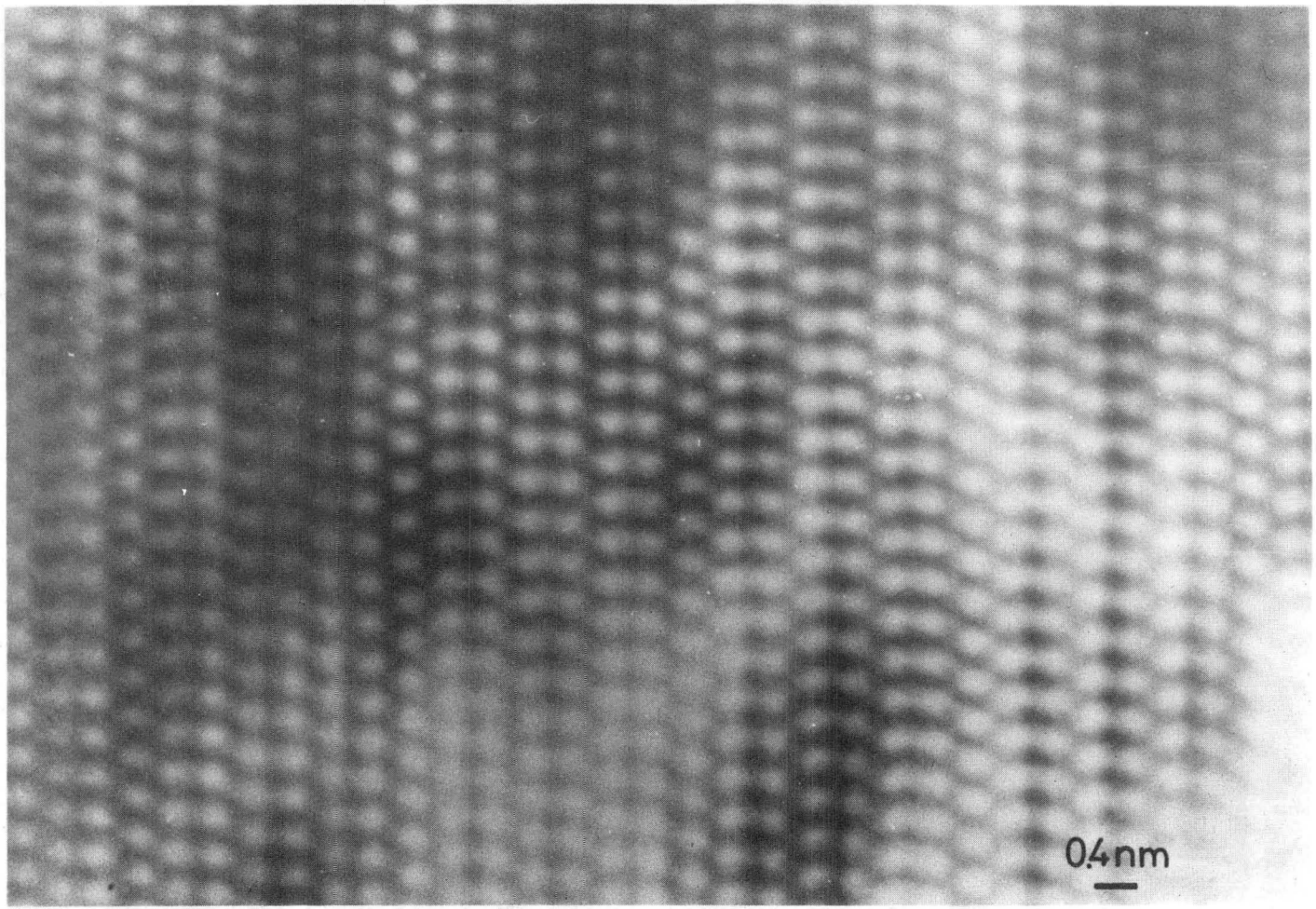

XBB 841 211

Figure 14.

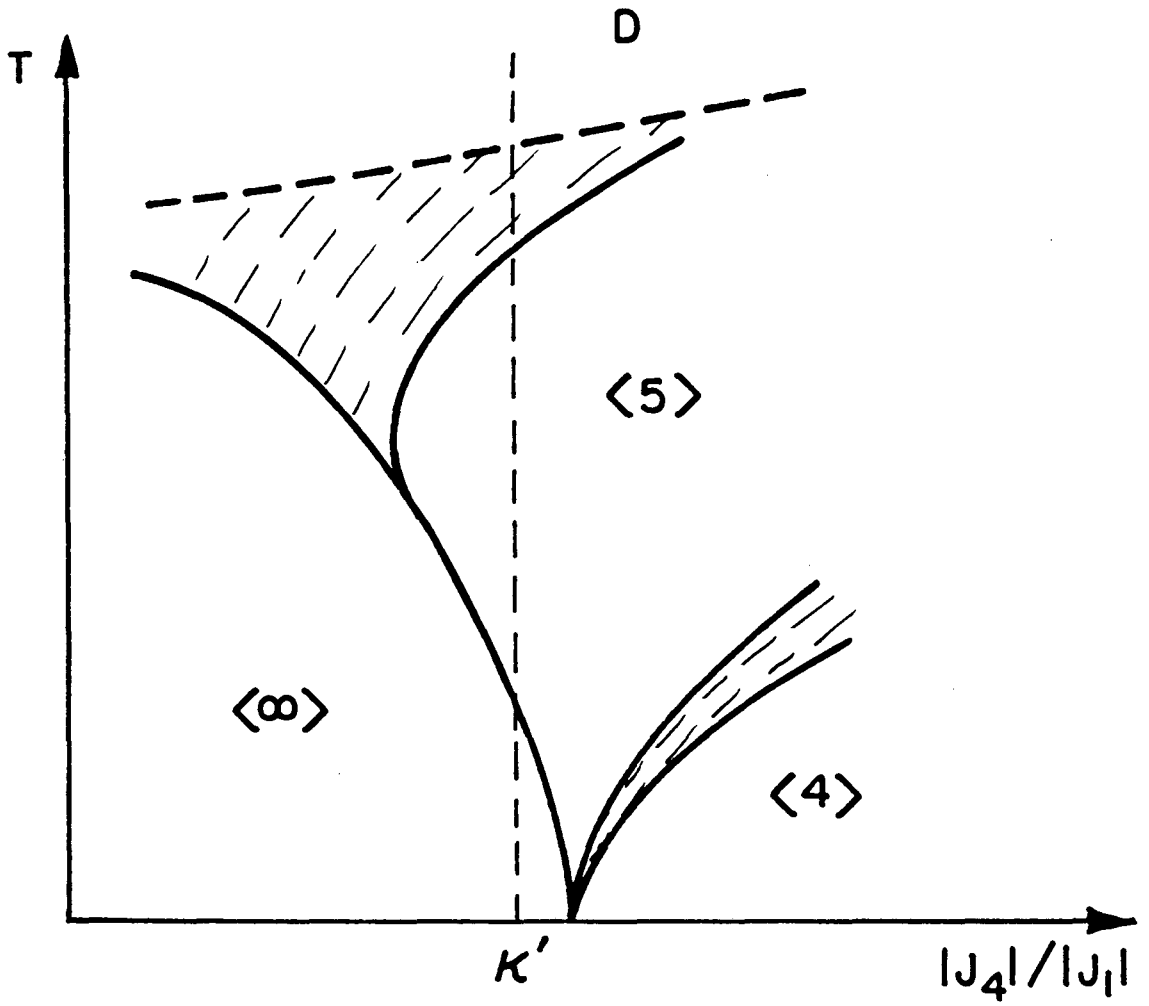

Figure 15.

XBL844-6870

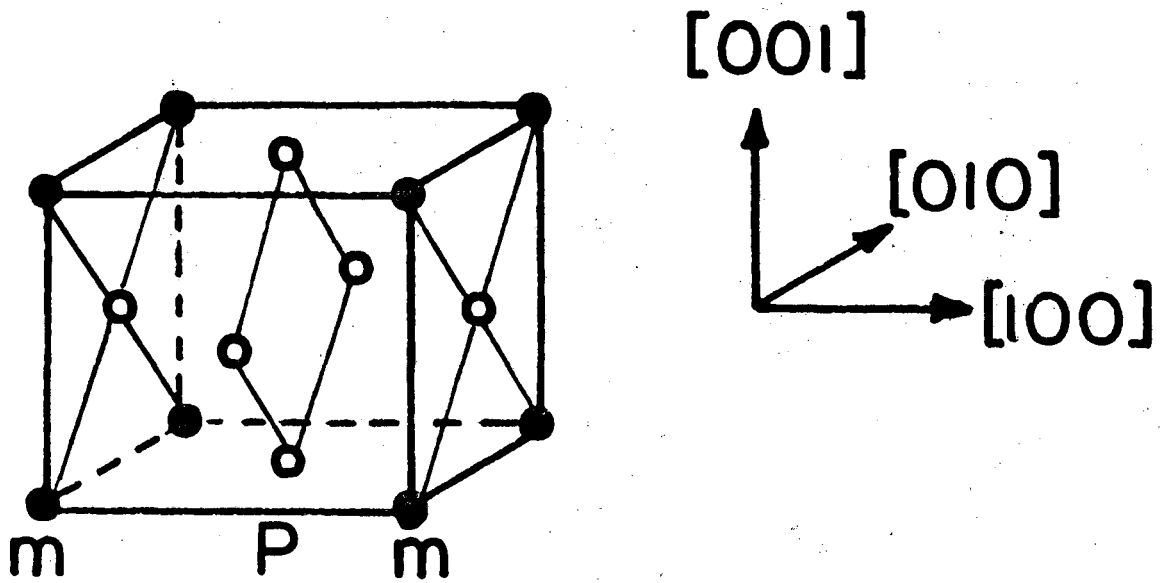

Figure 16.

XBL845-6951

This report was done with support from the Department of Energy. Any conclusions or opinions expressed in this report represent solely those of the author(s) and not necessarily those of The Regents of the University of California, the Lawrence Berkeley Laboratory or the Department of Energy.

Reference to a company or product name does not imply approval or recommendation of the product by the University of California or the U.S. Department of Energy to the exclusion of others that may be suitable.

TECHNICAL INFORMATION DEPARTMENT
LAWRENCE BERKELEY LABORATORY
UNIVERSITY OF CALIFORNIA
BERKELEY, CALIFORNIA 94720